UNIVERSITY OF SOFIA "ST. KLIMENT OHRIDSKI
FACULTY OF PHYSICS
DEPARTMENT OF METEOROLOGY AND GEOPHYSICS

A COMPLEX APPROACH TO THE RESEARCH OF ATMOSPHERIC AEROSOLS

DISSERTATION ABSTRACT

ON

VIKTORIA LYUBOMIROVA KLESHTANOVA

SOFIA, 2023

UNIVERSITY OF SOFIA "ST. KLIMENT OHRIDSKI
FACULTY OF PHYSICS
DEPARTMENT OF METEOROLOGY AND GEOPHYSICS

A COMPLEX APPROACH TO THE RESEARCH OF ATMOSPHERIC AEROSOLS

DISSERTATION ABSTRACT

ON

VIKTORIA LYUBOMIROVA KLESHTANOVA

For awarding the educational and scientific degree "PhD" in a specialty

4.1 Physical sciences – Meteorology

Scientist supervisor:

/Assoc. Prof., PhD V. Tonchev/

Head of Department:

/Assoc. Prof., PhD G. Guerova/

The dissertation student was enrolled as a full-time doctoral student (later the doctoral course was transformed into a correspondence form of study) at the Department of "Meteorology and Geophysics" of the Faculty of Physics at Sofia University "St. Kliment Ohridski" in the period 2019-2023. The dissertation has a volume of 111 pages. It consists of 10 chapters and a list of cited literature. Number of figures – 50. Number of tables – 7. Number of cited literary sources – 129, of which 7 internet sites.

The dissertation work was discussed and proposed for defense to an extended departmental council of the Department of "Meteorology and Geophysics" at the Faculty of Physics on 30.03.2023.

The defense of the dissertation work will be held on .....2023 from .... hours in the auditorium ..... of the Faculty of Physics, Sofia University "St. Kliment Ohridski", 5 "James Boucher" Blvd. The defense materials are available to those interested in the library of the Faculty of Physics of the Sofia University "St. Kliment Ohridski", 5 "James Boucher" Blvd.

I thank to:

my scientific supervisor Assoc. Prof., PhD Veselin Tonchev for the joint work, for the guidelines and help for the realization of the dissertation work,

Assoc. Prof., PhD Christo Angelov, INRNE-BAS, head of BEO Moussala, for providing the necessary data used in the dissertation work,

chief assistant PhD. Anastasia Stoycheva, NIMH, for help in preparing the synoptic analysis,

fellow forecasters from NIMH for their support and understanding over the years,

my whole family and all my loved ones for their patience and support.

Content

Chapter 1
Relevance and purpose of the dissertation work

1.1. Relevance of the problem

According to the latest sixth assessment report of Working Group I of the Intergovernmental Panel on Climate Change (IPCC) **[1]**, published in 2021, the aerosol contribution to the effective radiative forcing (ERF), the quantitative energy gained or lost by the Earth system after an imposed perturbation, decreased in magnitude from 2014 to 2019. The change over this period was estimated at +0.2 W/m^2. The contribution of aerosols to ERF has been estimated at –1.1 [–1.7 to –0.4] W/m^2 since the start of the industrial era, 1750. For comparison, the IPCC Fifth Assessment Report **[2]** estimates this impact at –1.3 [–2.0 to –0.6] W/m^2 for the period 1750–2014. Approximately 75-80% of this effective radiative forcing is due to interactions between aerosols and clouds. Aerosol–cloud interactions remain a major challenge in global numerical models due to limited knowledge of important submicron-scale processes, from aerosol emissions and their precursors to precipitation formation. Aerosols involved in aerosol-cloud interactions are called cloud condensation nuclei (CCN). It is their spatial and temporal distribution in the atmosphere that is of utmost importance to be able to include their effects in meteorological numerical models at all scales, from regional to global. CCN are studied by various methods all over the world – from point measurements or vertical profiles, through the search for direct relationships with atmospheric processes, to the study of regularities through empirically derived laws. Upper-atmosphere CCN measurements are often representative of free-atmosphere conditions. Therefore, the distribution of CCN along the mountain peaks is indicative of the transfer of air masses influencing the respective region. In Bulgaria, CCN have been counted since the end of 2015, when a CCN counter (CCNC) started functioning in the Moussala Basic Environmental Observatory in November. BEO Moussala is located on Mount Moussala, the highest mount in Bulgaria, as well as on the entire Balkan Peninsula, with an altitude of 2925 meters. In the dissertation work, the behavior of CCN was investigated, according to data from BEO Moussala in 2016. The research is the first of its kind on CCN in the territory of the country.

1.2. Purpose and tasks of the dissertation

The aim of the dissertation is to investigate for the first time the CCN in Bulgaria. The data are reported in BEO Moussala and are for the period from 1.01.2016 to 31.12.2016. The tasks related to this goal are:

1) Finding regularities in the distribution of CCN;

2) Determination and study of extremes (minimums and maxima) of the concentration of CCN;

3) Linking the distribution of CCN with different synoptic conditions and circulation features in the country;

4) Description of a nucleation system using known empirical laws.

Chapter 2

Current state of the problem

2.1. Aerosols

An aerosol is a collection of solid or liquid particles suspended in a gas phase. In the atmospheric sciences, however, the term aerosol is usually used in the plural to refer to "aerosol particles". Additionally, to distinguish cloud particles from other types of particles in the atmosphere, all hydrometeors (cloud droplets, ice crystals, raindrops, snowflakes, and sleet) are excluded from the definition of aerosols [3].

The amount of aerosols, as well as their properties, are diverse and variable in space and time. For this reason, aerosols can be divided according to several characteristics:

1) Regarding its source - primary and secondary [4].
2) Regarding their properties depending on the environment in which they are located [5] – urban (and their derivatives – semi-urban, rural), continental, desert, marine, volcanic, stratospheric.
3) According to their origin - natural and anthropogenic. From a climate perspective, the global radiation balance is affected by aerosols both directly and indirectly.

The ability of aerosols to absorb and scatter solar radiation determines their direct effect on climate. This leads to modifications of the vertical profile of shortwave radiative heating and atmospheric temperature. These changes account for the semi-direct effect of aerosols [6]. The indirect effect is due to the interaction of aerosols with clouds [7]. Aerosols change the

properties of clouds, incl. microphysical ones such as albedo, lifetime and precipitation structure. It has been proven that the increase in the number of aerosols, as a result of anthropogenic factors, leads to a decrease in the diameter of cloud drops and to an increase in cloud albedo, also in the lifetime of clouds, as a result of which precipitation decreases [8]**.** The interaction between aerosols and clouds is one of the biggest mysteries in modeling the effects of aerosols on climate.

2.2. Cloud condensation nuclei (CCN)

Aerosols involved in cloud formation are called Cloud Condensation Nuclei (CCN) [9,10]. The ability of aerosols to play the role of CCN depends on a number of factors. Mainly these are the supersaturation (S) of the surrounding air, the physical and chemical properties of the aerosols, as well as the meteorological parameters (eg temperature, pressure, humidity).

Cloud condensation nuclei can be clearly distinguished from aerosols by various measurements, as well as with the help of various numerical models, thanks to the advancement of technology and the development of improved methods for their simulation.

CCN cannot be measured directly. In order to account for them, indirect methods are used, which estimate the supersaturation of water vapor in the cloud. One way is by measuring the temperature gradient in a continuous flow of CCN counter (CCNC). Most often, cloud particles go through a series of cycles to reach the required supersaturation, usually on the order of 10 or more [11]. The particles are activated into cloud droplets at a certain pressure. For this reason, one interpolation is not sufficient to describe the entire spectrum of nuclei (droplets). Therefore, CCN are often compared across different meteorological parameters, such as temperature, relative humidity, wind direction and speed, precipitation [12].

Knowledge of the spatial and temporal distribution of CCN in the atmosphere is of utmost importance to be able to incorporate their effects into numerical weather models at all scales, from regional to global [26].

2.3. Aerosol-cloud interactions

Anthropogenic activity, especially the burning of biomass and fossil fuels, leads to a significant increase in emissions of aerosols and their precursors. In this way, elevated atmospheric aerosol concentrations have been reached since the pre-industrial era.

According to the sixth, final, assessment report of Working Group I of the Intergovernmental Panel on Climate Change (IPCC) **[1]**, published on 08/09/2021, the total

contribution of human activity to ERF from the beginning of the pre-industrial era to the end of the period examined in the report (from 1750 to 2019) is estimated at 2.72 [1.96 to 3.48] W/m^2. For the same period, aerosols have a negative total contribution to ERF of -1.1 [-1.7 to -0.4] W/m^2 *(***Figure 2.1***)*. About 75–80% of this ERF is due to aerosol–cloud interactions, with the remaining contribution due to aerosol–radiative interactions. In comparison, the IPCC's Fifth Assessment Report [2] estimates this impact at –1.3 [–2.0 to –0.6] W/m^2 for the period 1750–2014. This means that the change over the period 2014–2019, the subject of the IPCC Sixth Assessment Report, is estimated at + 0.2 W/m^2. Therefore, for these 5 years, the aerosol EW remains negative, but decreases in magnitude by 0.2 W/m^2. This is due to a reduction in global aerosol optical thickness and the reduction of aerosol emissions and their sources through a number of state and global regulations [14]. Based on these estimates, instead of suppressing warming, clouds will lead to an increase in the global radiation balance in the future, due to the release of more greenhouse gases and fewer aerosols into the atmosphere by human activities.

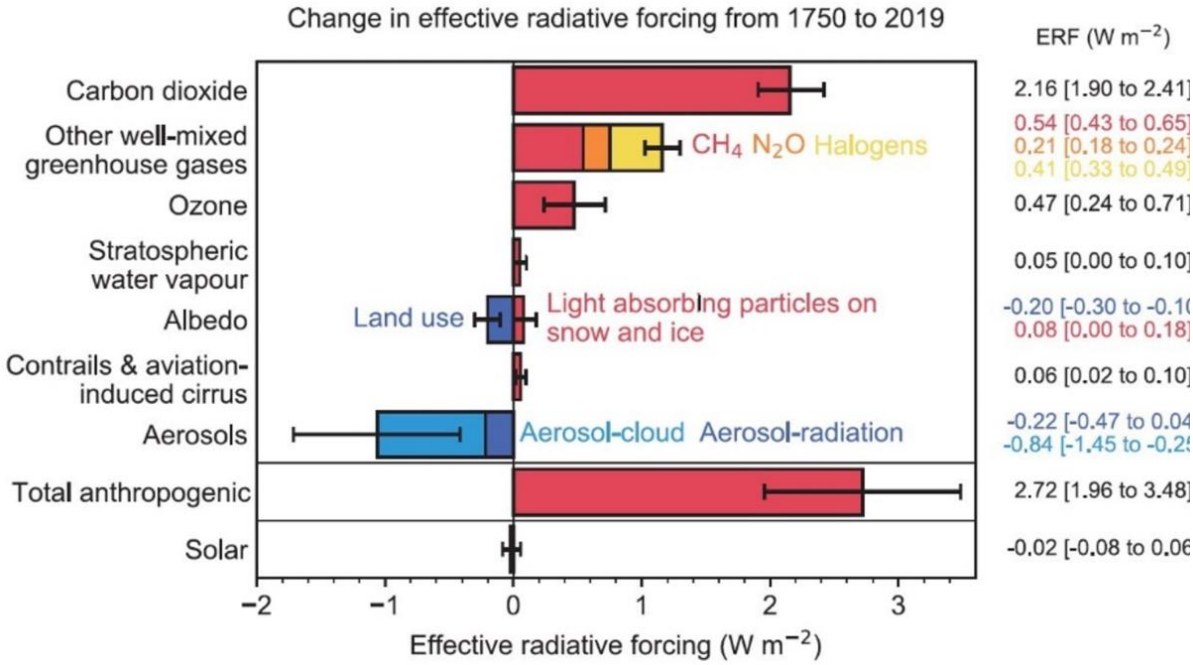

Figure 2.1: Change in effective radiative forcing from 1750 to 2019 by different types of sources marked on the left scale. Reproduced from IPCC **[1].**

2.4. Predicting the concentration of CCN

There are different ways to predict the concentration of OKA, but the most widespread and used methods are two. The first uses Köhler's theory [15] and is therefore more theoretically accurate. The second is through Twomey's famous empirical power law [16], which is also applied in the present dissertation.

2.4.1. Köhler's theory

The activation of CCN in cloud condensation processes was systematized by Köhler in 1923. Köhler's theory [15] describes the equilibrium vapor pressure of water above rising cloud drops. It is also used to determine if the drop is activated, ie. whether it has become a cloud drop or not and accordingly whether it will continue to grow spontaneously. The basis of Köhler's theory lies in all physically-based approaches describing the indirect effect of aerosols on the Earth's radiation balance [17]. Köhler's equation gives a basic equilibrium relationship between a drop of saline water and the water vapor above it:

$$\frac{e}{e_s} = a_{\mathrm{W}} \exp K_e = a_{\mathrm{W}} \exp\left(\frac{2\upsilon_{\mathrm{W}}\sigma_{\mathrm{sol}/\upsilon}}{RTr}\right), \qquad (2.1)$$

where e is the vapor pressure of water, e_s is the saturated vapor pressure of water, e/e_s =S is the compression coefficient, aw is the activity of water, Ke is the Kelvin coefficient, υ_w is the partial molar volume of water, $\sigma_{sol/\upsilon}$ is the surface tension tensor of the solution upon contact with the droplet, R is the universal gas constant, T is the temperature of the droplet, r is the radius of the droplet.

2.4.2. Twomey's empirical law

The most commonly used empirical formula for describing the dependence of CCN concentration (NCCN) on supersaturation (S) was proposed by Twomey [16]:

$$N_{CCN} = CS^k \qquad (2.3)$$

where the parameter C is equal to the number of activated CCN at S=1 and reflects the change in aerosol concentration [18]. Therefore, C has the largest values in polluted air and the smallest in clean air. The parameter k is dimensionless and represents the rate of change of CCN with the change of compression [19]. The two parameters have been used in the development of numerical models to predict cloudiness [20–22].

2.5. Other CCN studies worldwide

In the last few years, more and more studies of CCN are being done using different methods.

The changes in the size distribution of aerosols after the passage of a certain air mass have been studied, and a change in the microphysical and macrophysical characteristics of the clouds developed as a result of the particular situation has been determined [23]. Nilsson and co [24] suggest that the relationship between the microphysics and synoptics of the processes at these two different scales can be sought and explored through the meso-processes in the boundary layer.

Numerous studies have been done to find correlations between air mass backward trajectories and synoptic situations or individual meteorological parameters and elements, such as wind, clouds or precipitation, air mass moisture content, etc.[12,25–32]. They are also used in atmospheric chemistry, for example in pollutant tracking and ozone analysis and trace gas photochemistry [33]. Recently, the first studies of CCN have been carried out in many places in Europe, with the aim of detecting relationships between air masses and precipitation using backward trajectories.

2.6. Study of CCN on the Balkan Peninsula

In this section, an overview of the research on CCN during the last decade in the countries of the Balkan Peninsula is made. The area was chosen because it also includes the Moussala BEO. Using a bibliographic and reference database [34] 11 publications from Greece and 1 from Serbia were found and briefly described.

2.7. Study of CCN in Bulgaria

Data on OCJ in Bulgaria have been collected since the end of 2015 with the CCNC at the Base Environmental Observatory (BEO) Moussala, described in detail in Chapter 3. The first results of research on CCN in Bulgaria are part of the doctoral student's master's thesis and are presented by Kleshtanova et al in a 2019 publication. [35]. The article examines the distribution of CCN, as well as the dependence of this distribution on basic meteorological parameters - atmospheric pressure, temperature and relative air humidity.

2.8. Study of heterogeneous nucleation

In 1975-76, I. V. Markov and E. Stoycheva (Armyanova) from the Institute of Physical Chemistry at the Bulgarian Academy of Sciences investigated [36] the kinetics of nucleation of mercury on platinum cathodes under electrochemical conditions in which the driving force, superposition, is set by fixing the electrochemical potential (overpotential), in other words,

overvoltage, in the system. This is not the only possible approach to studying nucleation under electrochemical conditions. Another possibility is to set the rate of the electrochemical reaction, i.e. to fix the current [37]. When defining the driving force of the process in terms of overvoltage, the authors also note its analogue - gas-phase overpressure, in a separate article devoted to the theory of the phenomenon. The authors present the number of nuclei formed up to the time of counting as a function of time for 6 fixed overvoltages (overvoltages) - from 83 to 88 mV, figures 5 and 6 of Markov and Stoycheva [36]. Times are on the 10 millisecond scale.

The difference between the two figures is in the geometry of the cathode. A flat structureless platinum cathode was used to obtain the data in Figure 5. For the data in Figure 6, a single crystal platinum cathode in the shape of a hemisphere was used [36].

Chapter 3
Methodology and data sources

3.1. Basic Environmental Observatory Moussala

In 1959, on Mount Moussala, the highest peak of the Balkan Peninsula with an altitude of 2925.4 m (42° 10’ 45” N, 23° 35’ 07” E), a cosmic ray measuring station was built according to the idea of the prominent Bulgarian scientist Academician Georgi Nadjakov and the famous Hungarian physicist Academician L. Janoszy. In 1983, the station burned down. In 1999-2000, with the financial assistance of the Bulgarian "Ministry of Environment and Water", the station was reconstructed and renamed Basic Environmental Observatory (BEO) "Moussala" [38]. BEO Moussala is a part of the Institute for Nuclear Research and Nuclear Energy (INRNE) of the Bulgarian Academy of Sciences.

3.1.1. CCN counter

In this thesis, the CCN data used are reported by the Cloud condensation Nuclei Counter, which is part of the BEO Moussala aerosol measurement system.

The size of the range of activated particles, i.e. per CCN, is measured in microns and ranges from 0.75 μm to 10 μm, and particles are distributed into 20 bins (size intervals, “bins”). In the first box, particles with sizes up to 0.75 μm fall, in the second box, particles with sizes from 0.75 μm to 1 μm are grouped. The width of the boxes is then 0.5 μm (1.0 – 1.5 μm, 1.5 – 2.0 μm, ..., 9.5 – 10.0 μm). CCN concentration is measured per cubic centimeter (#/cm^3).

At any given moment, CCNC operates on a single overshoot. In BEO Moussala, six different compressions are used, 0.13; 0.23, 0.43, 0.53, 0.73 and 1.13% which change automatically every 10 minutes. The column has three temperature control zones along its walls, with the temperature increasing from the top to the bottom zone.

The concentration of CCN (#/cm^3) was obtained for each day of the year 2016.

3.2. Backward trajectories of air masses

In order to trace the origin and characteristics of the air masses influencing the amount of CCN, and to find connections between them, their backward trajectories were calculated.

In the current dissertation, the HYSPLIT model was used to obtain the backward trajectories of the air masses [39].

Backward trajectories were calculated for the BEO Moussala territory using the geographic coordinates of Mt. Moussala described above. The chosen duration of the trajectories is 72 hours, as this time interval very well describes the development of atmospheric processes and the path of air masses on the continent of Europe.

The backward trajectories used in this thesis are divided by several features that well describe the path of the air masses over the Balkans: On the one hand, relative to the underlying surface, sea (S) or continental (C), of the air masses. For this purpose, it is subjectively counted in each hour what type of subsurface the relevant air mass is above. Three subgroups are defined:

a) When the air mass is more than half and less than 75% of the time, ≥36<54 hours, over the continent (C) or over the sea (S) is additionally marked with “a”.

b) When the air mass is for 75% or more hours of the time, ≥54 hours, over the continent or over the sea is additionally marked with “b”.

c) When the air mass is all the time, 72 hours, over the continent or over the ocean is additionally marked with "c".

Air masses move in layers of the atmosphere of different thickness and altitude. In relation to them, the following division of trajectories is made: high (high, H) are those that, during their movement, reach an altitude above 4500 meters; medium (medium, M) are those that move in a layer with an altitude between 1500 and 4499 meters; low (low, L) are those that have passed through a layer of the atmosphere with an altitude below 1499 meters.

In order to find connections with the applicable operational practices used in the National Institute of Meteorology and Hydrology in Bulgaria, a grouping of the trajectories of

advective and non-advective part was done by Stefanov et al. [40]. According to this classification, the advective (cyclonic) lobe has 4 subtypes: Atlantic (Atl), Mediterranean (Med), Continental (Cont) and anticyclonic type (Low gradient pressure (LGP)). Each of the advective subtypes has subtypes marked with numbers, all of which are detailed by Stefanov et al. [40].

There are three types of Atlantic (ocean) advection: subtype Atl1 – oceanic advection by cyclone, subtype Atl2 – oceanic advection by anticyclone, subtype Atl3 – mixed type of oceanic advection under the combined influence of cyclone and anticyclone. Continental advections are divided into: subtype Cont1 – advection of continental air masses from the northwestern and northern sectors, subtype Cont2 – advection of continental air masses from the northern and northeastern sectors, subtype Cont3 – advection of continental air masses from the northeastern sector, Cont4 – advection of continental air masses from the eastern and southeastern sectors. Mediterranean advections are described in detail by Stoev and Guerova [41]. Non-advective (anticyclonic) parts are divided into anticyclonic type (AC) - winter and summer anticyclone, as well as gradientless baric field.

3.3. Analysis of synoptic situations

To illustrate the analysis of the synoptic situation, the maps from the Global Forecasting System (GFS), atmospheric reanalysis maps, which are a combined product of the National Centers for Environmental Prediction (NCEP) and the National Center for Atmospheric Research (National Center for Atmospheric Research, NCAR) of the United States, as well as data from NIMH on wind direction and speed, (NCEP/NCAR Reanalysis).

The analysis itself was prepared following established long-standing operational practices, updated with modern methods for describing synoptic processes used in the Meteorological Forecasting Department of NIMH.

NCEP/NCAR reanalysis [42] are based on the period 1981 - 2010 and were calculated at a height of 700 hPa, using the average value for the geopotential and its anomaly from the average value for the period under consideration.

3.4. Jenkinson-Collison-Types classification

The Jenkinson-Collison-Types (JCT) atmospheric circulation described by Stoev et al. [43], presented in **Figure 3.1** was used to group different characteristics related to CCN concentration. The classification includes: 1) eight main directions, west (W), southwest (SW),

northwest (NW), north (N), northeast (NE), east (E), southwest (SE) and south (S), 2) one cyclonic type (C) and 3) one anticyclonic type (AC). There are also two additional groups: 1) eight anticyclonic types (AW, ASW, ANW, AN, ANE, AE, ASE, and AS) and 2) eight cyclonic types (CW, CSW, CNW, CN, CNE, CE, CSE, and CS). The most common types were extracted from the typology and compared with data from air mass backward trajectories obtained from NOAA's HYSPLIT model.

F

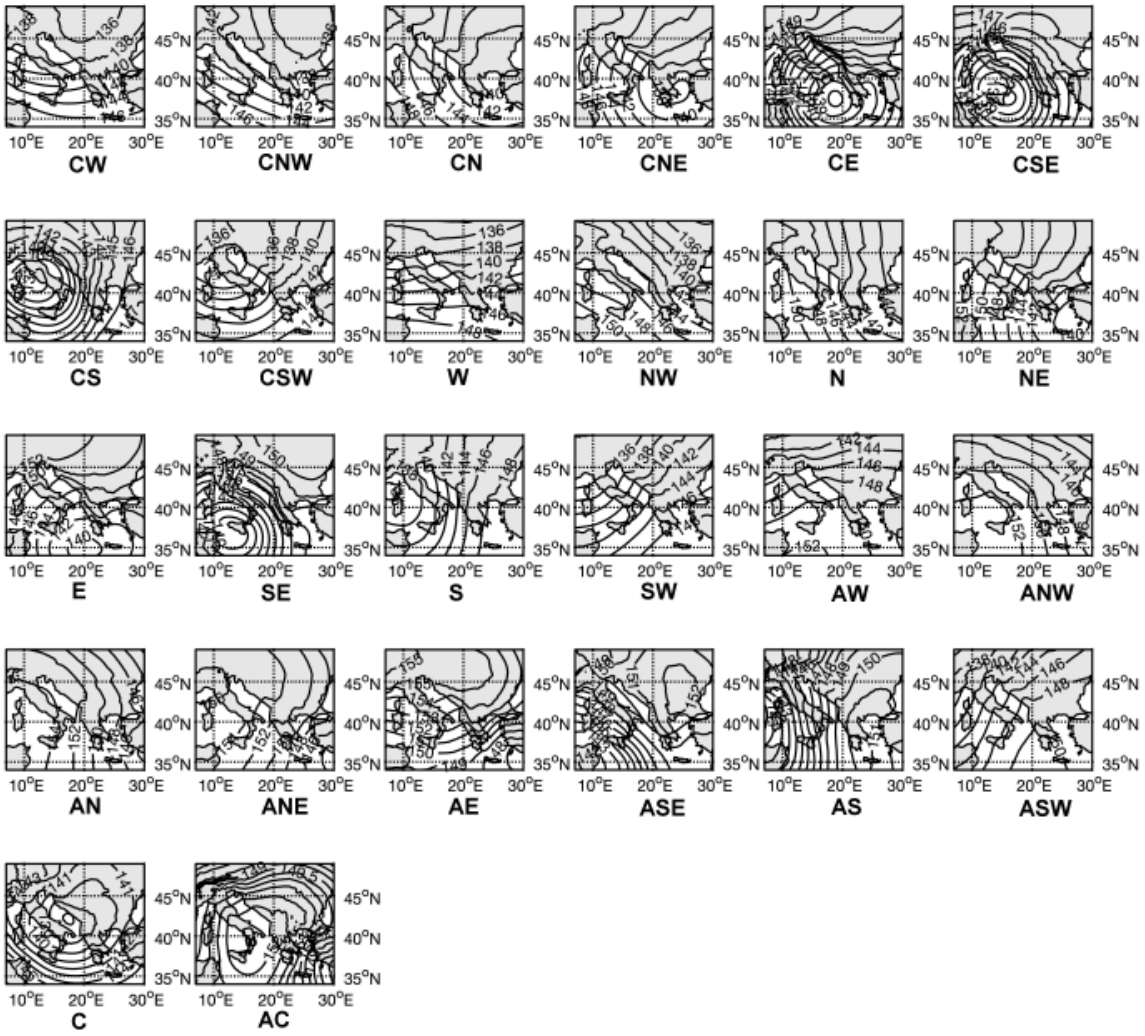

Figure 3.1: JCT circulation diagram with 26 circulation types. Reproduction by Stoev and collective [43].

Chapter 4
CCN distributions and relation to two synoptic situations in 2016.

4.1. CCN distribution in January 2016 and analysis of the synoptic situation at the end of the month

The diurnal trend of CCN concentration in January 2016, reported in BEO Moussala and presented by Kleshtanova et al. [35], shows 4 situations with CCN concentrations above 400 counts per cubic centimeter. From these situations with maximum concentrations of CCN, one was selected, the only one, which has two extremes of concentration very close to each other, in the period 29-31.01.2016, presented at Figure 4.1. It shows that the extreme values of the CCN concentration were recorded in the afternoon hours, on the 29th and 31st, respectively. On the 30th there is another extremum, but more than twice as small as the other two.

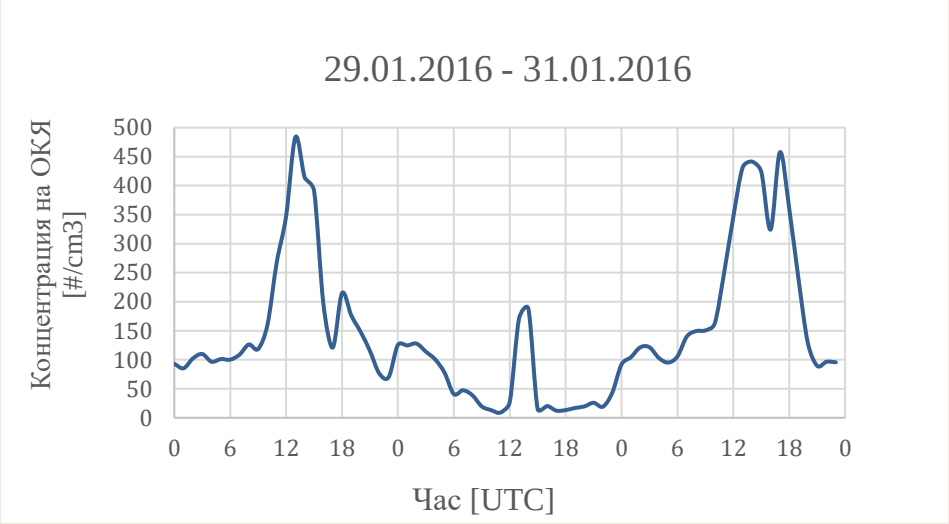

Figure 4.1: Distribution of CCN by hours on 29.01.2016 – 31.01.2016 г.

Absolute topography (AT) maps at 700 hPa (AT700) show that when the CCN numbers extrema (29th and 31st afternoon) the geopotential over the country is still relatively high, ***Figure 4.2****, a)* and *e),* higher on the 29th, with a downward trend on the 31st, with the baric topography having more of a cyclonic curvature characteristics, which is also evident from the 500 hPa isobaric surface on both days, respectively **Figure 4.2**, *b)* и *f).* The baric field at a height of 700 hPa on 29/01/2016 at 12 UTC is low-gradient, relatively high, with a shallow baric valley approaching the country, which is also well defined at the 500 hPa isobaric surface, **Figure 4.2**, *a)* and *b).* During the night of the 29th to the 30th, the baric valley crossed the country. In the morning hours of the 30th, the formation of a ridge begins from the west, the axis of which crosses the country by noon, and the ridge is well distinguishable at both geopotential heights **Figure 4.2**, *c)* и *d).* At 12 UTC, a smaller, compared to that of the 29th and 31st, CCN extremum was reported.

700 hPa 500 hPa

29.01

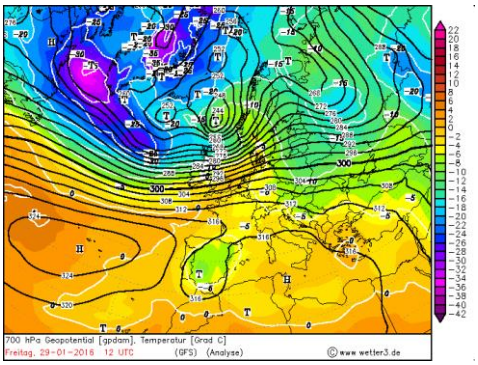

a)

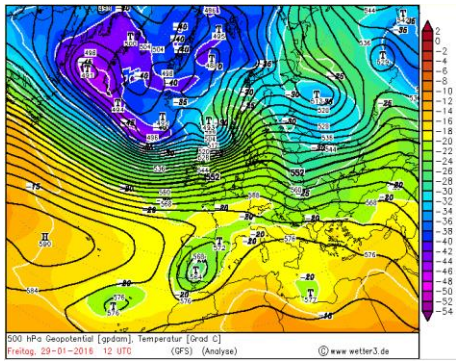

b)

30.01

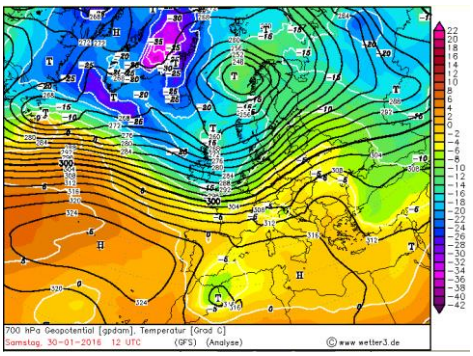

c)

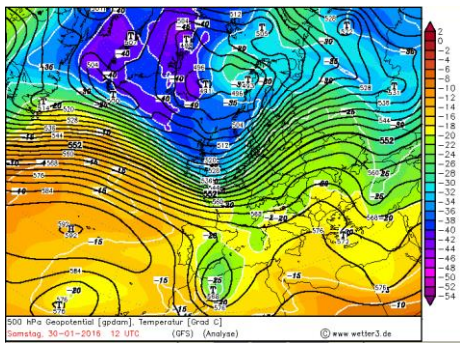

d)

31.01

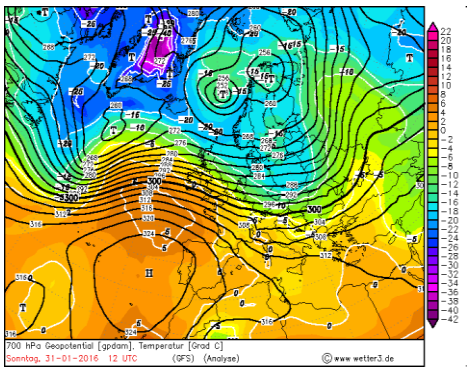

e)

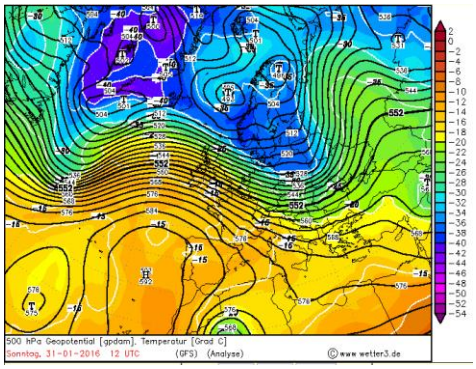

f)

Figure 4.2: Geopotential at 700 hPa on 29, 30 and 31.01.2016 at 12 UTC, respectively *a)*, *c)* and *e)* and at 500 hPa for the same days, respectively *b)*, *d)*, and *f)* [44].

At night, the crest is destroyed and on 31.01.2016 the country is again under the influence of a baric valley associated with a cyclone with two main centers: one - over the northern part of the Scandinavian Peninsula and the second - west of the coast of Norway, over the Atlantic Ocean. The geopotential is decreasing, but remains relatively high. The baric field is now more gradient, the wind is increasing, the flow at 500 and 700 hPa (**Figure 4.2**, *e)* and *f)*) is predominantly westerly, the cyclone centers are far to the north, and the Balkans are in the broad gradient frontal zone of the vast valley.

The increased baric gradient during the considered period, 29-31.01, leads to strong wind, the reported speed is up to 14 m/s from the west and west-northwest according to NIMH data (**Figure 4.3**, *a)*). A strong wind was also recorded from the northeast. The predominant direction of the wind is the southwest - up to 9 m/s. The data from the NIMH synoptic station, which is also located on Mt. Moussala, are in all synoptic time periods – 00, 03, 06, 09, 12, 15, 18, 21 UTC. The BEO Moussala (Automatic Weather Station VAISALA) instrument gives direction and speed information every 10 minutes (**Figure 4.3**, *b)*). According to the instrument readings there, there are no west wind registrations. The predominant directions that are preserved are northwest and southwest and a speed above 15 m/s.

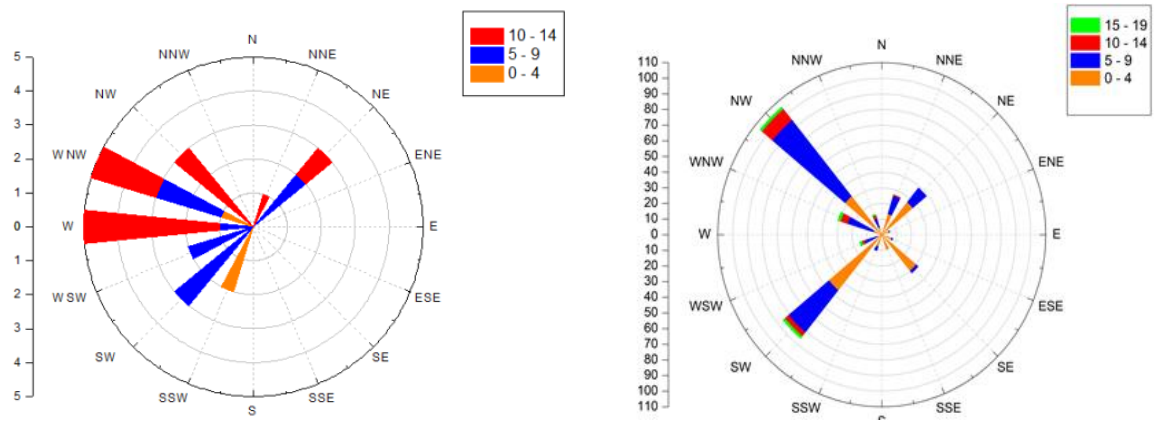

a) b)

Figure 4.3*:* Wind rose for the period from 01/29/2016 at 00 UTC to 01/31/2016 at 21 UTC according to a) NIMH and on b) BEO Moussala. The scale on the left refers to the width of the circles in the rose. Each round counts the number of repetitions at a given speed.

The relative humidity of the air at the beginning of the situation (January 29, 2016 around noon) in most of the country is between 60 and 75%, only over Southwestern Bulgaria it is up to 30-45% (**Figure 4.4**, *a)*). After 12 UTC on 29/01/2019 the relative humidity decreased to about 30% and did not change until the afternoon hours of 31/01/2016 when it started to rise from the northwest (**Figure 4.4**, *b)*).

Visibility in this setting is high. According to data from NIMH measurements during most of the period (in 20 of the 24 considered synoptic terms it is between 60 and 75 km), in 4 synoptic terms (on 29.01 21 UTC, 30.01 00 UTC, 31.01 18 UTC and 21 UTC) visibility was reported between 0 and 100 m, due to fog.

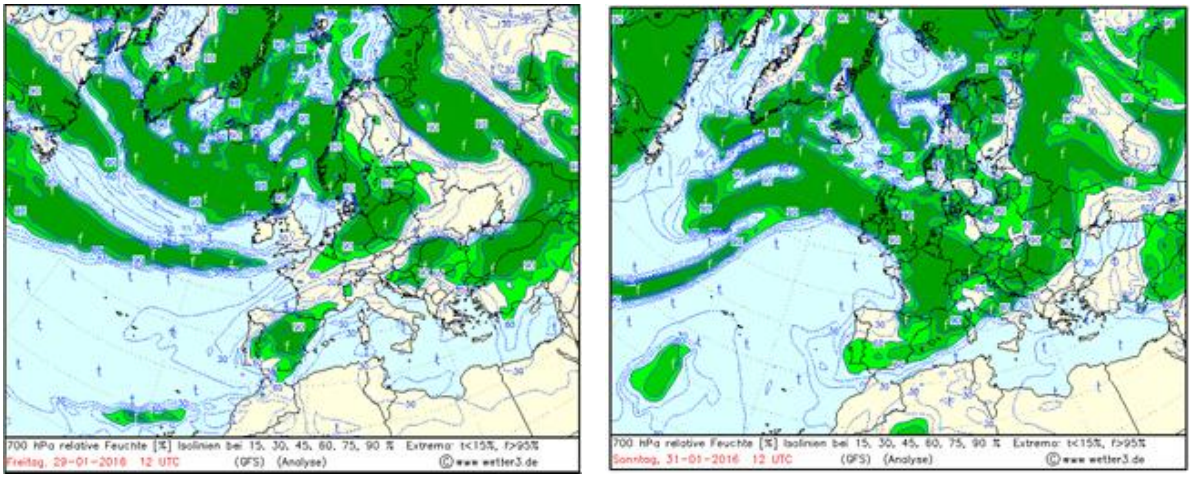

a) b)

Figure 4.4: Relative air humidity at 700 hPa at *a)* 29.01.2016 at 12 UTC and on *b)* 31.01.2016 at 12 UTC (to the right) [44].

The summer situation in the period was analyzed similarly 12-13.07.2019.

Chapter 5

CCN and backward trajectories of air masses at Mount Moussala

5.1. July and December 2016 CCN features

Using the renormalization procedure:

$$n_d = \frac{Nd}{N} 100\% \quad (5.1)$$

where N_d is the number of OCs of size d and N is the total number of CCN in the same volume [45], it is shown that it maps the renormalized distributions into an (almost) universal one. The distribution of CCN for each day of the month of July is presented at **Figure 5.1** at supersaturation of the air: *a)* 0.13%; *b)* 0.23%; *c)* 0.43%; *d)* 0.63%; *e)* 0.83%; *f)* 1.03%. To represents the percentage of the given size out of the total as a function of size. The distribution for December was investigated similarly.

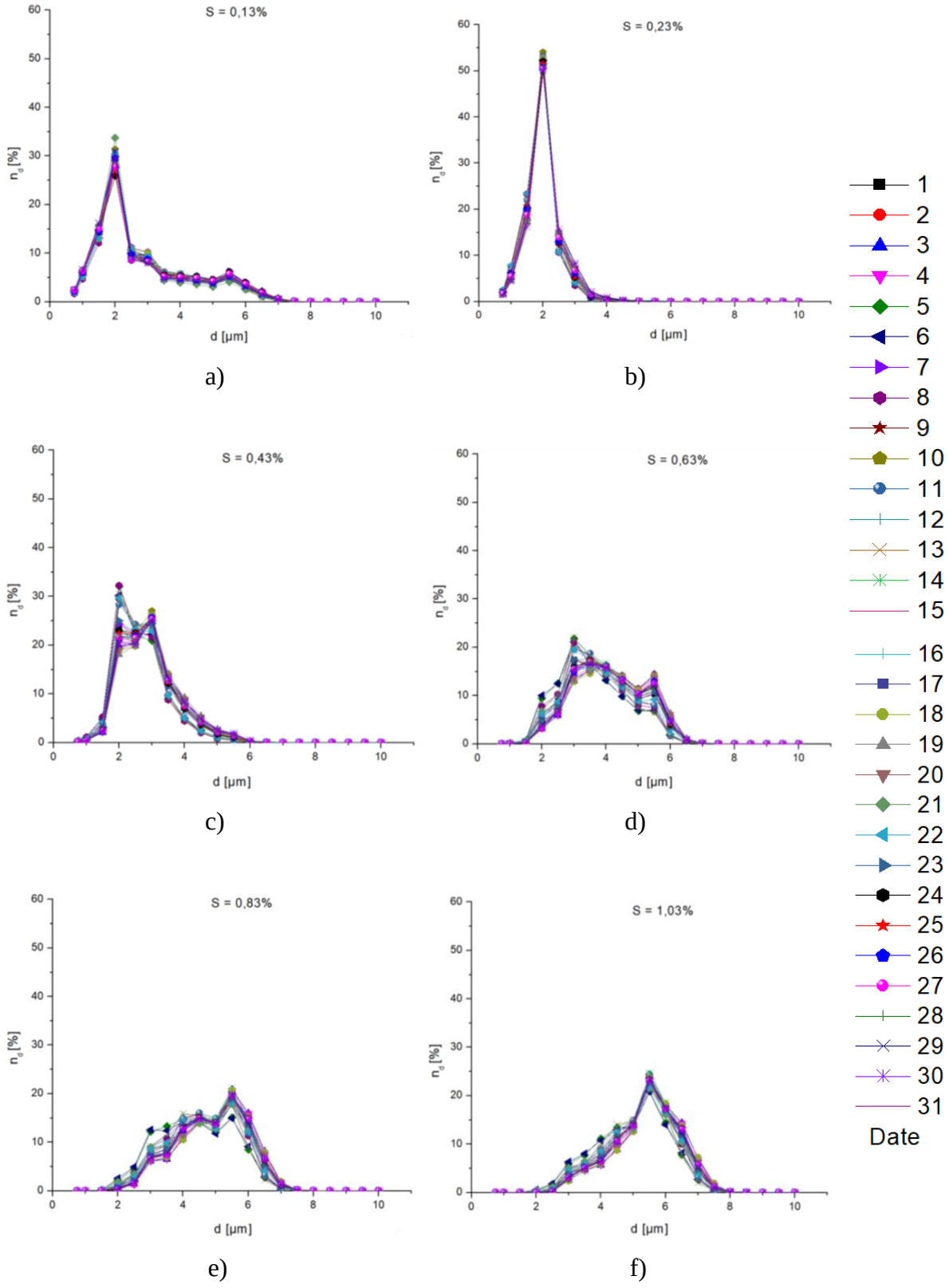

Figure 5.1: Distribution of CCN at a given supersaturation: *a)* 0.13%; *b)* 0.23%; *c)* 0.43%; *d)* 0.63%; *e)* 0.83%; *f)* 1.03% in July 2016. Each curve represents a specific day noted on the legend to the right.

The transformation, the division of N in equation 5.1, brings the distributions to a universal form, as mentioned at the beginning of this chapter.

At air supersaturation S = 0.13% and S = 0.23%, (**Figure 5.1**, *a)* and *b)* the most common diameter of CCN is 2 μm; at S = 0.43% (**Figure 5.1**, *c)* this maximum remains, but a second, smaller one appears at 3 μm. In the other three air pressures used 0.63%, 0.83% and 1.03%, respectively for July **Figure 5.1**, *d), e), f)* the 2 μm peak is not detected, but peaks for the 3 μm and 5.5 μm sizes are observed.

The concentrations of CCN are presented separately for each of the air pressures used, on a mean diurnal scale for the two months considered, July and December 2016, respectively at **Figure 5.2**, *a)* and *b)*. The Oy-axis is chosen equal, so the figure shows that kernel concentrations are significantly higher in July than in December. In addition, there are days with peak concentrations in both months. In July these are the 5th, 6th and 13th, and in December: the 2nd, 6th and 12th. In July, there is a clear minimum concentration - on the 18th. In the summer month, the concentration of CCN is about 4-5 times higher for extremes than in winter. Some reasons can be hypothesized for the differences between July and December: (i) July reports more pollutants, including pollen and also as a result of large fires in agricultural areas; (ii) Saharan dust transport is more intense in July; (iii) In July, differentially warmed mountain slopes at the summit create conditions for the initiation of a local mountain-valley breeze that lifts some local aerosols.

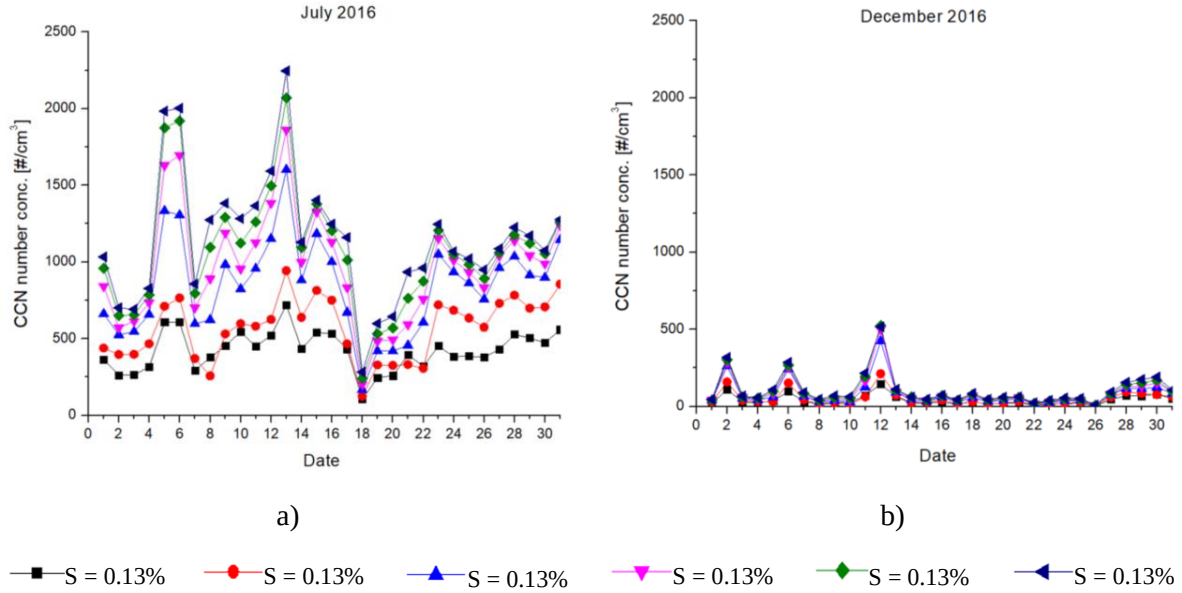

Figure 5.2: CCN concentration in July *a)* and *b)* December, at the various interpolations used, shown with a general legend below the figures.

5.2. Influence of air masses of Mount Moussala

Air masses in July and December 2016 affecting Mount Moussala derived from NOAA's HYSPLIT model backward trajectories are grouped by several features. First, on **Figure 5.5**, *a)* and *b)*, a grouping of the concentration of OKA was made according to the thickness of the atmospheric layer in which the air mass moves during the last 72 hours, before reaching BEO Moussala. Atmospheric layers are divided into:

- High (H) > 4500;
- Medium (M) [1500-4499];
- Low (L) [0 - 1499].

In July 2016 (**Figure 5.3**, *a)*) the influence of trajectories reaching Moussala from the higher atmospheric layers prevailed (a total of 17 days), followed by those from the lowest layers (9 days), and the least number of days were those in which the Mt. Moussala was affected by air masses coming from the middle atmospheric layers (5 days). In December 2016 (**Figure 5.3**, *b)*) the influence of air masses coming from the lowest layers of the atmosphere prevailed (13 days), followed by the influence of the upper layers (10 days), and for the remaining 8 days, Moussala was affected by air masses coming from the middle layers.

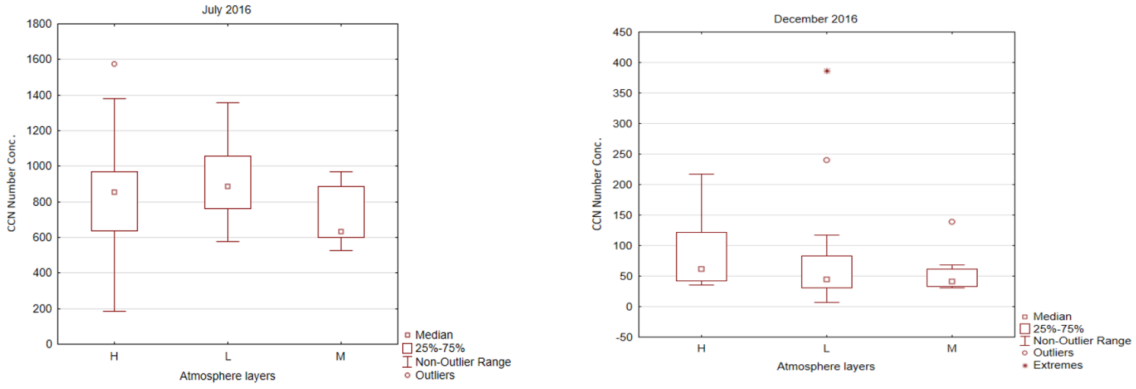

a) b)

Figure 5.3: Concentration of CCN clustered with respect to the atmospheric layers obtained from the backward trajectories by month a) July and b) december 2016 г. In each box with whiskers, the distribution is reported by: square – median; rectangle – interquartile range; the two dashed ends enclose the range that is not outside the limits of the distribution; circle – outlier.

The second grouping of the concentrations of CCN is according to the types of weather that affect the atmospheric circulation over Bulgaria [40]. According to this classification, the advective (cyclonic) part has 4 subtypes: Atlantic (Atl), Mediterranean (Med), continental (Cont), and anticyclonic type (Low gradient pressure (LGP)). Each of the advective subtypes

has subtypes marked with numbers, all of which are described in detail by Stefanov et al [40]. These are precisely three types of Atlantic (oceanic) advection: subtype Atl1 - oceanic advection by cyclone, subtype Atl2 - oceanic advection by anticyclone, subtype Atl3 - mixed type of oceanic advection under combined influence of cyclone and anticyclone. The continental advections are divided into: subtype Cont1 - advection of continental air mass from the northwest and north sector, subtype Cont2 - advection of continental air mass from the north and northeast sector, subtype Cont3 - advection of continental air masses from the northeast sector, Cont4 - advection of continental air masses from the eastern and southeastern sector. The Mediterranean advections are described in detail by Stoev and Guerova [41]. All advective subtypes are outlined, and an approximation of the Mediterranean advections is presented. The non-advective (anticyclonic) parts are divided into anticyclonic type (AC) - winter and summer anticyclone, as well as a gradient-free baric field.

In July 2016 (**Figure 5.4**, *a)*) the most frequently occurring type was Atl2 (11 days) with an average CCN concentration of 844 #/cm^3, while the least reported type was Cont1 with a concentration of 578 #/cm^3. In December 2016 (**Figure 5.4**, *b)*) the most frequently occurring type was Cont1 (7 days) with an average CCN concentration of 101 #/cm^3, and the least reported type was LGP-c, observed only on one day with a concentration of 57 #/cm^3.

The third grouping is based on the length of time that air masses spend over the adjacent surface, described in detail in Chapter 3, section 2. In both months, continental (C) air masses predominate - 30 days in July and 21 days in December. However, in December, the median concentration of C air masses is 47 #/cm^3, while that of sea (S) air masses is 57 #/cm^3. In July, on the other hand, practically all trajectories are continental, with the exception of one day.

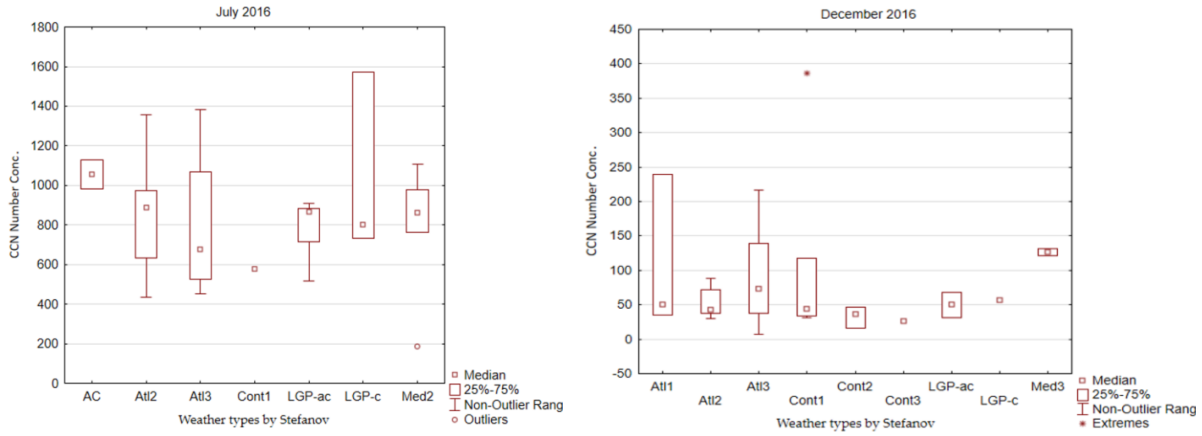

a) b)

Figure 5.4: CCN concentration grouped by the Stefanov classification obtained from the backward trajectories by month *a)* July and *b)* December 2016 г.

In each box with whiskers, the distribution is reported by: square – median; rectangle – interquartile range; the two dashed ends enclose the range that is not outside the limits of the distribution; circle – outlier.

5.3. Meteorological Data

NCEP/NCAR reanalysis data show that in July, the mean geopotential value over northern regions of Europe is cyclonic with a cyclone center between Iceland, the British Isles, and Norway. In the remaining parts, including Bulgaria, the mean geopotential field is anticyclonic (**Figure 5.5**, *a)*). In December, at the 700 hPa pressure level, Eastern Europe and the Balkan Peninsula are under the influence of a baric trough. The mean geopotential over the rest of Europe is anticyclonic (**Figure 5.5**, *b)*).

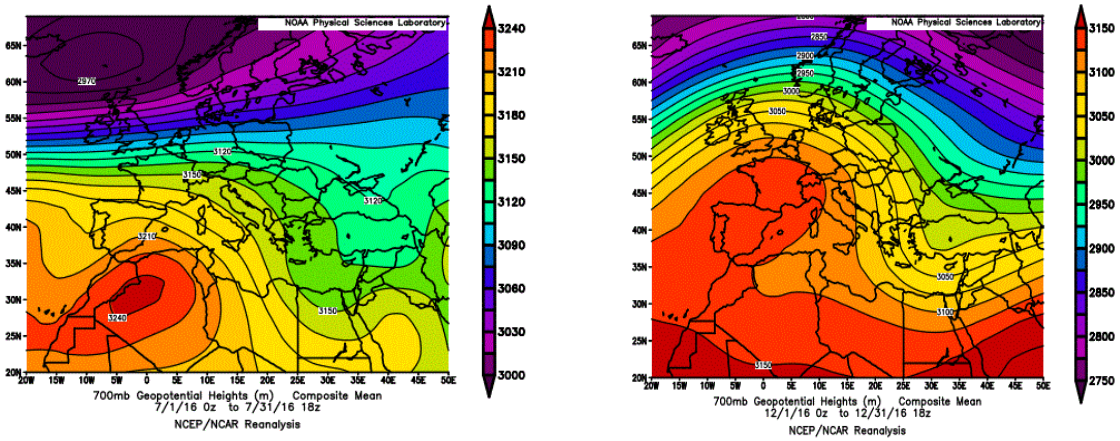

a) b)

Figure 5.5: Average geopotential height at 700 hPa isobaric height (hPa), 1981-2010 NCEP/NCAR reanalysis for *a)* July and *b)* December 2016, [42].

In July, over most regions of Europe, including Bulgaria, the temperature anomaly at the 700 hPa pressure level is positive: between 0.3 K (Kelvin) and 1.5 K. Negative temperature

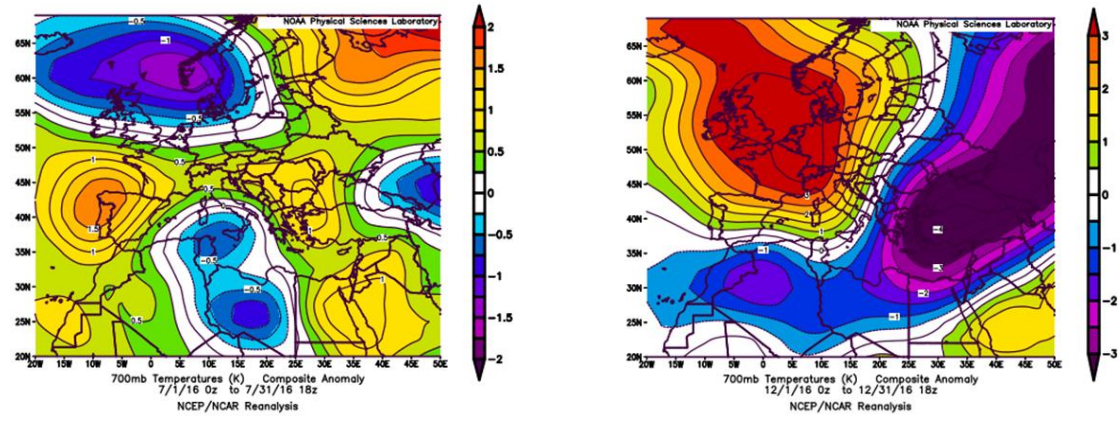

a) b)

Figure 5.6: Temperature anomaly at isobaric height 700 hPa, 1981-2010 NCEP/NCAR reanalysis for a) July and b) December 2016, [42].

anomaly occurs over Scotland, southern parts of the Scandinavian Peninsula, and the central Mediterranean Sea (**Figure 5.6**, a)). In December, over the Balkan Peninsula, Asia Minor, the Black Sea, and southern parts of European Russia, the temperature anomaly at 700 hPa is negative: from 1 K to over 3 K. Over the rest of Europe, the temperature anomaly at 700 hPa is positive (**Figure 5.6**, b)).

5.4. Extreme concentrations of CCN

As shown **Figure 5.7** *a),* there are four extremes in the distribution of air pollutant concentrations in July. These are the 5th, 6th, treated as one synoptic situation, and 13th (maxima), and the 18th (minimum). In December, there are three clear maxima on the 2nd, 6th, and 12th, **Figure 5.2**, *b).*

The NCEP/NCAR reanalysis for July shows that during the maximum concentrations of air pollutants (5th, 6th, 13th), the mean geopotential value at 700 hPa over Bulgaria has an anticyclonic curvature or is gradient-free, while during the minimum of air pollutants (18th), the mean geopotential at 700 hPa is cyclonic, and Bulgaria and the entire Balkan Peninsula are affected by a baric valley. The temperature reanalysis for July shows that on the 5th and 6th, there is no temperature anomaly over Bulgaria, while on the 13th it is positive, and on the 18th it is negative.

In December, during all days with maximum concentrations of air pollutants, the Balkan Peninsula is affected by a baric valley at 700 hPa. The temperature anomaly is negative in the first two cases. For the last one, the temperature anomaly over Southwest Bulgaria, where Mt. Moussala is located, is positive, while over Northeast Bulgaria, the temperatures are around their average values.

The behavior of the wind has also been studied and wind roses for the examined days have been plotted **(Figure 5.7**). The wind data is from the NIMH station at the Mt. Moussala for all synoptic times (main and intermediate) - 00, 03, 06, 09, 12, 15, 18, 21 UTC. When the weather is calm, these hours are not accounted for on the roses. In July, on the days with observed maximum concentration (**Figure 5.7**, *a), b)*), the wind is mainly northwesterly, moderate, with speeds up to 9 m/s. During the observed minimum (**Figure 5.7**, *c)*), a strong north-northeasterly wind was recorded in one of the time periods, which is probably the reason for the low concentration of nuclei on that day. In December, the concentration of OCPs is significantly lower than in July. Strong and gusty winds were recorded during all reported maximums, with winds reaching up to 29 m/s in one of the dayss (**Figure 5.7**, *d), e), f)*).

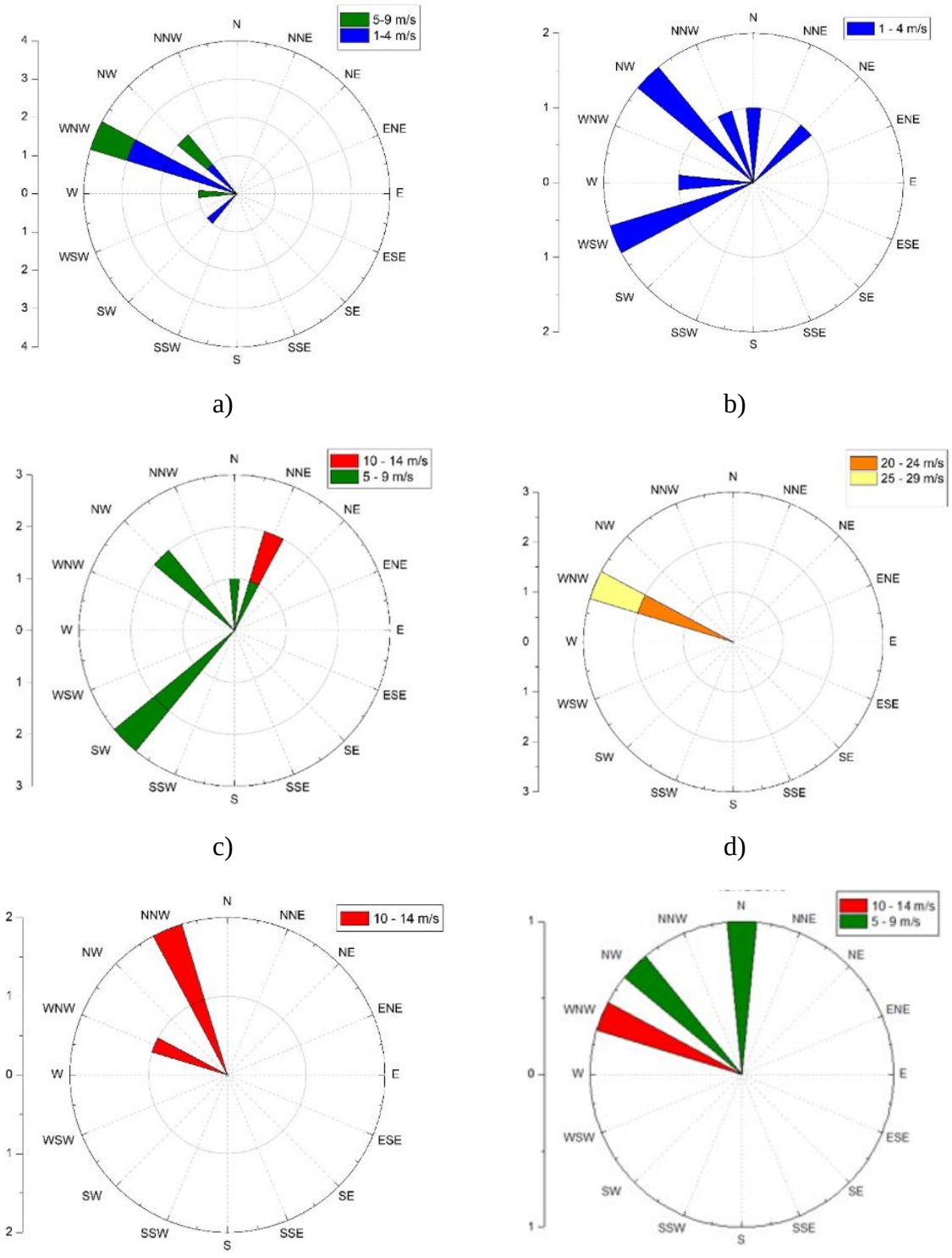

Figure 5.7: Wind roses on *CCN* extreme days. In July: a) *5-6*, b) *13*, c) 18 during December*:* d) *2*, e) *6*, f) *12*. Each round counts the number of repetitions of the corresponding direction. In some terms, data is missing or there was no wind.

Chapter 6

Extremes in the concentration of atmospheric pollutants and their relation to automatic synoptic classification of atmospheric processes in 2016.

6.1. Concentration of CCN on a daily average scale in 2016

For the purposes of this study, the concentration of CCN is averaged on a daily average scale with a supersaturation of 0.43% for each day of 2016, and days with extremely high and extremely low concentrations are separated. Their number is summarized in **Figure 6.1**, *a)*. The least number of days with extremely low values occurs in December (zero days), while with extremely high values - in July and September (two days each). The most cases with extremely low values occur in March, May, and October (five days each), and with extremely high values - in May (six days). These days with extremely low or extremely high concentrations of CCN are grouped according to the types of atmospheric circulation of JCT, shown in **Figure 6.1**, *b)*. From the figure, it can be seen that extremely low concentrations of CCN are most frequently recorded in C, NW, and W types of atmospheric circulation, with 10, 9, and 5 cases, respectively, while extremely high concentrations are observed in SW, W, and NW types, with 8, 7, and 6 cases, respectively. That is, both types of extremes are observed in W and NW JCT types but differ in the third most frequently reported type of atmospheric circulation of JCT. This third type is the absolute maximum for the corresponding type of extreme: C for the lowest values of CCN concentration, and SW for the highest. In addition, in cases of extremely high CCN concentrations, only one case of C type is reported (maximum for extremely low values), while in cases of extremely low CCN concentrations, no cases of SW circulation type are reported (maximum reported many times for extremely high values). In cases of maximum high concentrations, in addition to the three main types of atmospheric circulation, three secondary types can also be determined - AW, N, and NE, each with three reported cases.

a)

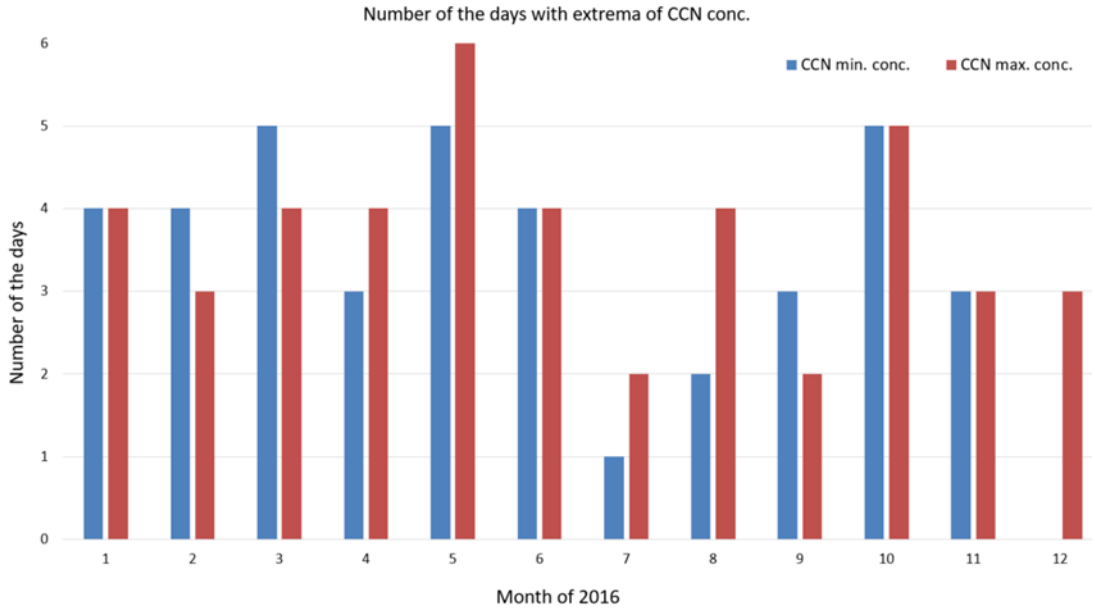

b)

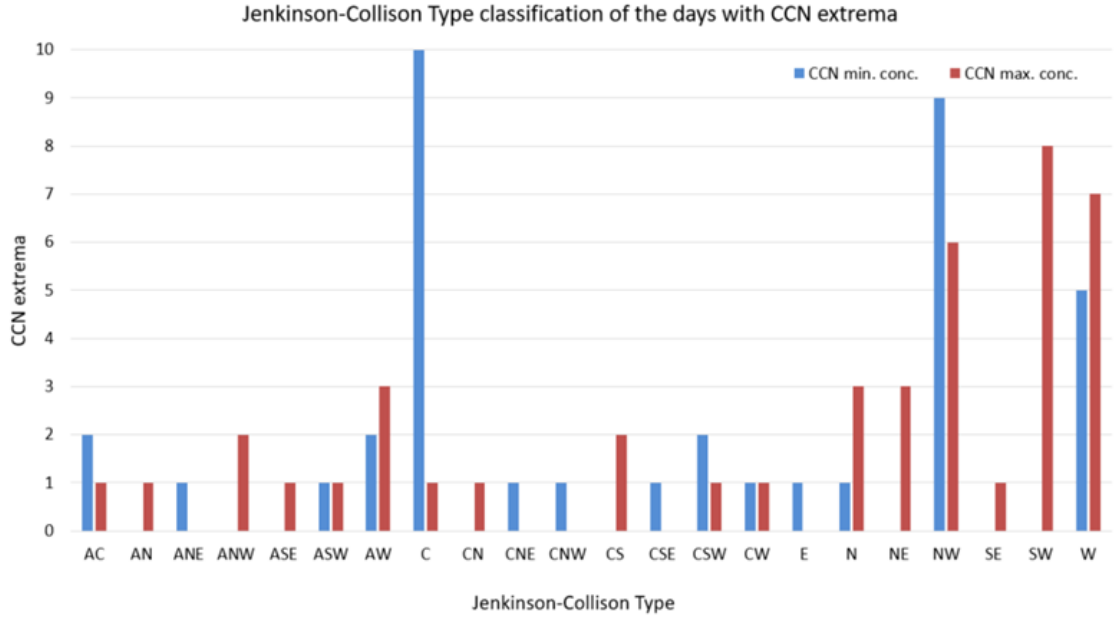

Figure 6.1: Monthly distribution of the number of days in 2016 c a) extreme low (blue bars) and high (red bars) values of CCN concentration and b) JCT circulation types.

6.2. Concentration of CCN on an hourly scale in 2016

In this study, the CCN concentration at S=0.43% is averaged for each hour for each recorded minimum and maximum. The days with minimums are represented by box plots in **Figure 6.*2***, labeled on the legend to the right. The days with maximums are also investigated within the dissertation. There are no extreme minimum values of CCN concentration in December.

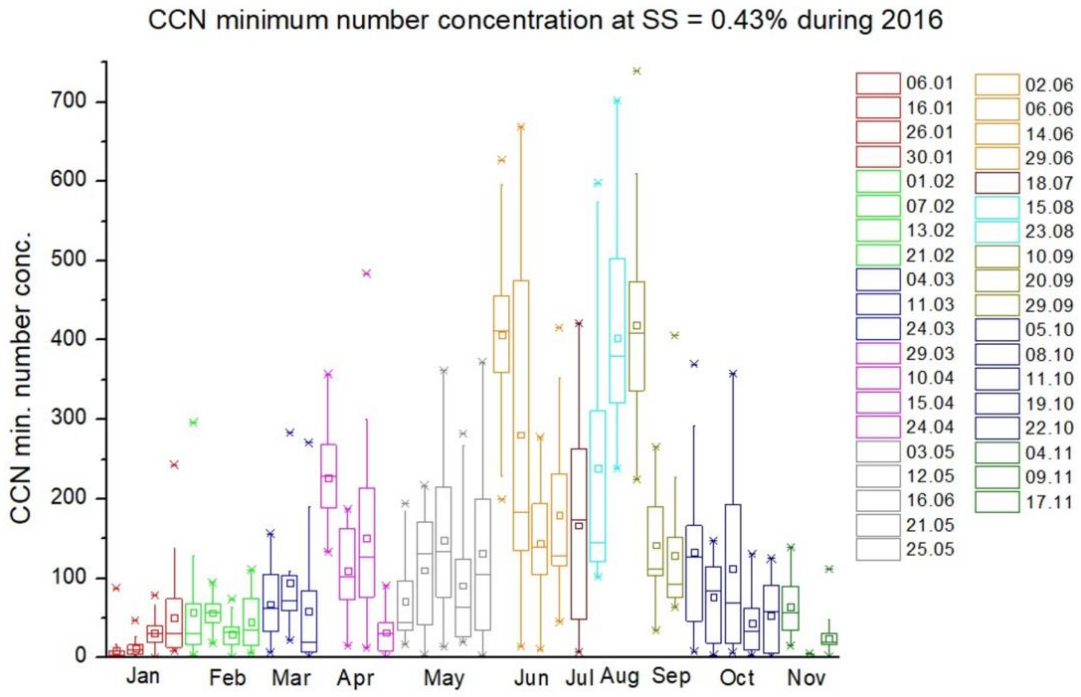

Figure 6.2: Concentration of CCN on an hourly scale for all days with reported minimum values. The legend on the right indicates the specific day. Different colors correspond to different months, represented along the x-axis.

In **Figure 6.2** each box represents the distribution of data for a specific day with reported minimum values. The central line represents the median, the square represents the mean, and the rectangle represents the interquartile range. The 5th and 95th percentiles are indicated by whiskers, and the minimum and maximum values are represented by crosses. During the studied period in 2016, there were 38 cases with extremely low concentrations of air pollutants and 44 cases with extremely high concentrations. Generally, the concentration of air pollutants is higher during the summer than in winter.

6.3. Distribution of days with extremes using HYSPLIT

For each day with a reported minimum or maximum concentration of PM10, a backward trajectory is plotted using the HYSPLIT model. The selected duration of the trajectory is 72 hours back, as this period of time describes well the path of air masses over Europe and the development of atmospheric processes that affect the Balkan Peninsula. The backward trajectories reach the peak of Moussala every day at 12 UTC. The model provides information on the location, geographic coordinates, and altitude of the air mass at each hour. Two types of grouping have been made. On the one hand, according to the underlying surface, sea (S) or continental (C), of the air masses. For this purpose, it has been subjectively counted in each

hour over what type of underlying surface the respective air mass is located. Three sub-groups have been identified:

a) When the air mass is over the continent or over the ocean for more than half and less than 75% of the time, ≥36<54 hours, it is marked with "a".

b) When the air mass is over the continent or over the ocean for 75% or more of the time, ≥54 hours, it is marked with "b".

c) When the air mass is over the continent or over the ocean for the entire duration of 72 hours, it is marked with "c".

Using this classification, the most frequently occurring typologies of atmospheric circulation according to JCT obtained in point 6.2 were compared. For extremely low values of the concentration of CCN, these are C, NW, and W, and for extremely high values - C, NW, and W. From **Figure 6.3** it can be seen that for extremely low values of the concentration of VOCs, under atmospheric circulations of type C and NW, a prevailing type of the origin of the air mass can be determined, namely Sa (a maritime air mass, which spends between 36 and 54 hours over the ocean and the rest over the continent) and Cc (a continental air mass, which spends the entire 72 hours over the continent). For atmospheric circulation of type W, there is no prevailing origin of the air mass. The same applies for extremely high values of the concentration of CCNs.

Another type of grouping of air masses, which is again obtained from backward trajectories calculated through the HYSPLIT model, is based on altitude, which is aligned with the basic atmospheric layers used in synoptics. Three groups of air masses have been identified based on the maximum altitude they pass through:

a) Low (L) - up to 3000 meters (= 700 hectopascals, hPa), which is very close to the altitude of Mount Moussala (2925 meters);

b) Medium (M) - up to 5500 meters (= 500 hPa, mid-tropospheric layer);

c) High (H) - above 5500 meters.

Comparing the altitude of air masses with their origin determined above, it can be seen that extremely low concentrations of air pollutants cannot be linked to a specific dependence between altitude and their origin. With this type of grouping, during days with minimal concentrations of air pollutants, it is not possible to determine the predominant relationship between atmospheric layer and origin of air masses.

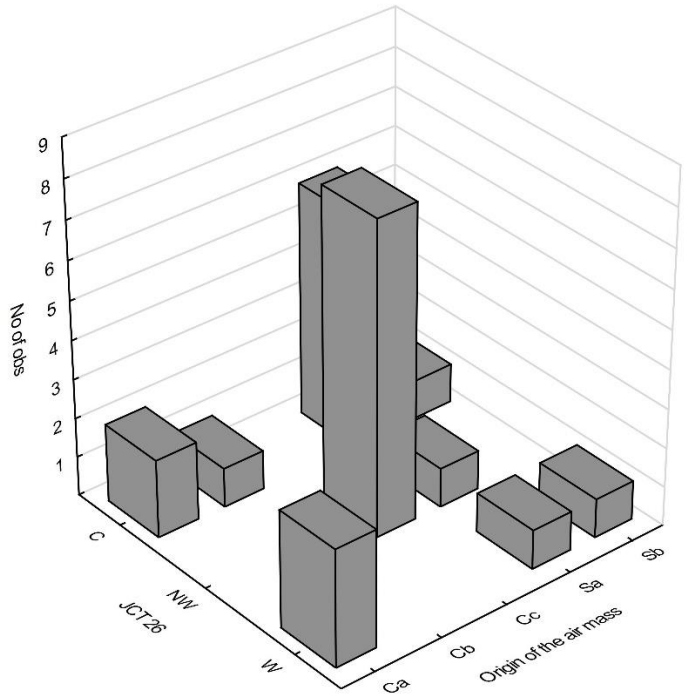

Figure 6.3: Two-dimensional histograms on the origin of air masses versus the JCT classification during the days with minimal concentrations of CCN's.

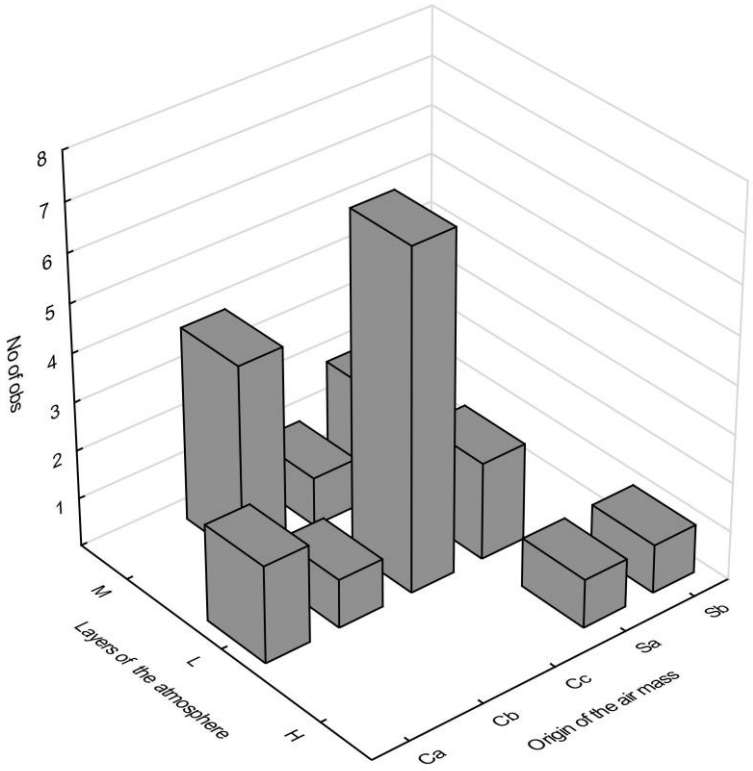

Figure 6.4: Two-dimensional histograms on days with maximum CCN for the origin of air masses versus JCT classification.

At extremely high concentrations of CCN, the opposite is true. There is no clear relationship between JCT classifications and the origin of the air masses, but the two most common air masses are: (1) one that comes from the low layers (L) and is purely continental (Cc) and (2) one that comes from the middle layers of the atmosphere (M) and has spent more than 75% of the time over the continent (Cb), as shown in **Figure 6.4**.

CHAPTER 7
Application of Twomey's law

Twomey's law [16], $N_{CCN} = CS^k$ (equation 2.3), and its use on a global scale are described in detail in Chapter 2, section 2.4.2. Here, NCCN is the number of CCN per cubic centimeter, S is the supersaturation, and C and k are parameters. The parameter C is equal to the number of activated CCN at S=1% (#/cm^3), and the parameter k is dimensionless and represents the rate of change of CCN with changes in supersaturation.

7.1 Approximation of CCN

The data for the CCN distribution are "fitted", i.e. an acceptable approximation is made using Twomey's law at the six saturation levels used by the CCN instrument: 0.13%; 0.23%; 0.43%; 0.63% and 1.03%. Four months from 2016, February, May, August, and November, representing spring, summer, fall, and winter, were selected. In February, the CCN instrument was configured by the manufacturers [46] to measure only at 5 saturation levels, with 0.13% missing. The approximation was obtained for each day of the considered period for the minimum, maximum, and mean daily values of CCN concentration in BEC Moussala. There are missing approximations for individual days where, due to technical reasons related to the CCN instrument, CCN concentration was not measured. In addition to the approximation, the table presents data obtained from the software, such as the name of the model used (Twomey), the form of the equation (c*S^k), the date, the values of the sought parameters, C and k, and their standard error, as well as basic statistical characteristics such as the adjusted coefficient of determination R2 (Adjusted R Square) and reduced Chi-Square.

As a result of the approximation of the daily average, minimum and maximum concentrations of CCN, the obtained R^2 is relatively high for each approximation.

7.2. Dependency of parameters C and k on temperature

In an attempt to find a dependency of parameters C and k, obtained by approximation with Twomey's law (equation 2.3), basic meteorological characteristics were used, such as temperature, wind direction and speed, relative humidity, atmospheric pressure. As a result, the most suitable dependency was obtained with respect to temperature - minimum, maximum and average daily values. Temperature data are from the synoptic station Moussala (catalog number 15615, altitude 2925 m) and the climate station Borovets (catalog number 64225, altitude 1350 m) and are available in all synoptic terms - 00, 03, 06, 09, 12, 15, 18, 21 UTC. Borovets climate station was chosen for comparison because of its location at the foot of Mount Moussala. Borovets is located 10.3 km north of Moussala in a straight line. In November 2016, following a tragic incident, the Moussala synoptic station was temporarily preserved and data was not available.

Figure 7.1 shows the parameters C and k obtained from the approximation of the average daily concentrations of CCN, compared with the corresponding average daily (T_{avg}) temperature for the month of August from a) the Moussala synoptic station and b) the Borovets climatic station, respectively, on each of the figures. Direct and inverse proportional dependencies, as well as displacement between the two characteristics, are observed.

An example of this is shown in **Figure 7.2**, where the distribution of parameter C is shifted 24 hours forward (17-22.08.2016) compared to the distribution of maximum temperature (16-21.08.2016) in Borovets. The figure shows a similar trend in both characteristics. Figures similar to **Figure 7.2**, are plotted to represent the identical trend of parameters from Twomey's equation and temperature, where the actual trend of parameter C (#/cm^3) for the period 17-22.08.2016 and the maximum temperature in Borovets for the period 16-21.08.2016, shifted by 24 hours, are presented to demonstrate their identical behavior. Similar results have been obtained for different time periods during the four months examined, both at the Mt Moussala and in the resort of Borovets. This leads to the need to find a physical explanation for the behavior of the parameters obtained from Twomey's law and subsequently to separate characteristic time periods. The study generates new research questions that can be the subject of future additional research.

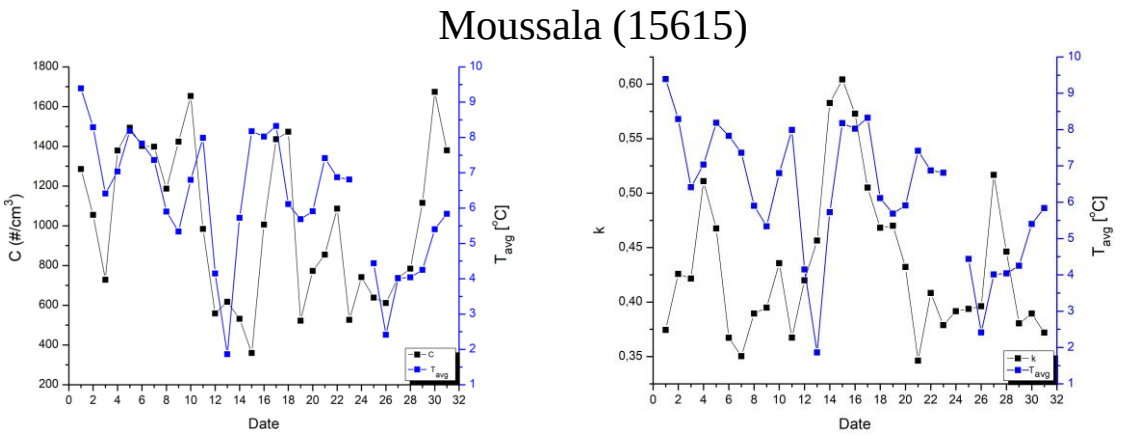

a)

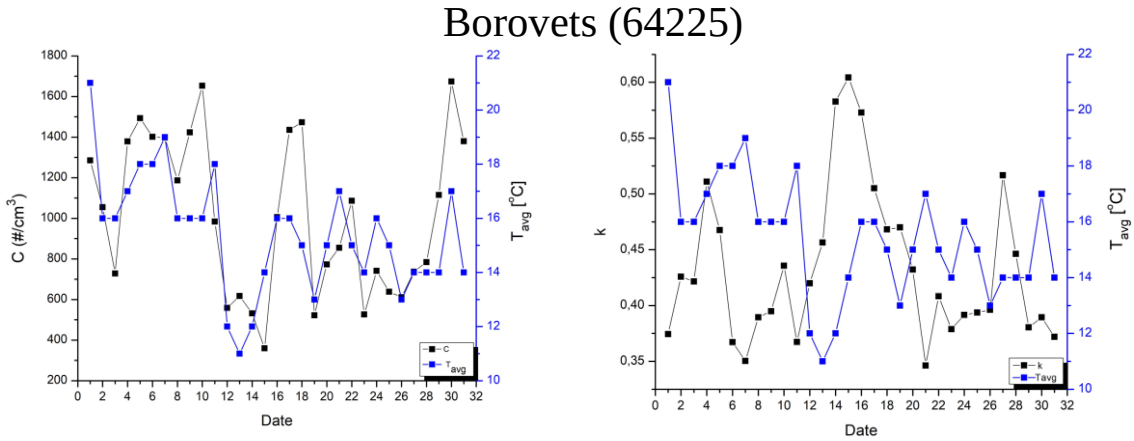

b)

Figure 7.1: The parameters C (#/cm^3) and k (dimensionless) obtained from the approximations of the daily average concentrations of PM10 using the Twomey law and the daily average temperatures from a) Moussala synoptic station and и b) Borovets climate ctation.

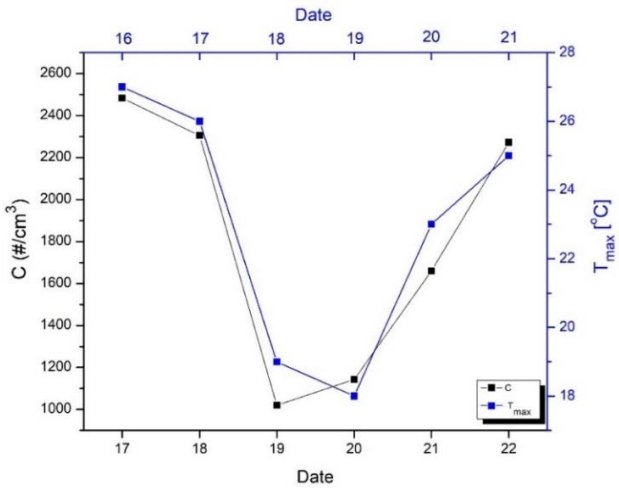

Figure 7.2: Dependency of parameter C (#/cm^3) for the period of 17-22.08.2016, obtained from the approximation of maximum CCN concentrations with respect to the maximum temperature in Borovets for the period of 16-21.08.2016.

7.3. Correlation coefficient between parameters C and k and temperature

After establishing a uniform behavior of the parameters from Twomey's law and the temperature, the JCT classification scheme described in Section 3.5 [43] and already applied in Chapter 6 was used.

For each day of the four examined months (February, May, August, and November 2016), respectively winter, spring, summer, and autumn, the Pearson correlation coefficient [47] was calculated. Based on it, the possible correlations in percentages [%] are [48]:

- 0.90 до 1.00 (−0.90 до −1.00): Very high positive (negative) correlation;
- 0.70 до 0.90 (−0.70 до −0.90): High positive (negative) correlation;
- 0.50 до 0.70 (−0.50 до −0.70): Medium positive (negative) correlation;
- 0.30 до 0.50 (−0.30 до −0.50): Low positive (negative) correlation;
- 0.00 до 0.30 (0.00 до −0.30): Unsatisfactory correlation.

During the study period, 12 types of circulation were recorded, each of which occurred for at least 4 days. Circulations reported up to three times, including during the study period, were disregarded due to the inability to properly calculate the correlation coefficient.

Overall, the correlation coefficient between temperature and parameter C is higher than the correlation coefficient between temperature and parameter k. The correlation coefficient for Moussala between temperature and parameter C shows a very high positive correlation in 8 cases and a very high correlation in 11 cases out of all possible 36. The correlation coefficient

for Borovets between temperature and parameter C shows a high positive correlation in 17 cases and a very high correlation in 9 cases out of all possible 36. The difference in the number of reported circulations in **Table 7.1** is due to the temporary conservation of the Moussala meteorological station in November, following a tragic incident.

The most common types of weather circulation during the studied period are anticyclonic (AC) and western (W) circulation types according to the JCT. The correlation coefficient is calculated for 10 days for Mt. Moussala and 18 days for Borovets during AC circulation type. During W circulation type, the correlation coefficient is calculated for 13 days for Mt. Moussala and 18 days for Borovets.

The highest correlation coefficient (0.995%) is obtained between the maximum temperature at Mt. Moussala and parameter C under CW circulation type, which occurs 4 times during the studied period. Under the same conditions, the correlation coefficient for Borovets is 0.972%.

Table 7.1: Correlation coefficient between the parameters from the Twomey equation obtained from the maximum concentrations of air pollutants and maximum temperatures at the Moussala and Borovets peaks for the entire study period (May, February, August, November 2016).

JCT	Number of obs.	Moussala correl. coef. [%]		Number of obs.	Borovets correl. coef. [%]	
		Tmax_*c*	Tmax_ *k*		Tmax_c	Tmax_k
AC	10	0,762	-0,178	18	0,840	-0,279
ASW	4	0,916	-0,168	5	0,947	-0,073
C	4	0,923	-0,603	9	0,717	-0,281
CW	4	0,995	-0,747	7	0,972	-0,714
N	4	0,577	-0,572	5	0,772	-0,616
NW	4	0,634	0,760	6	0,564	-0,381
S	4	-0,879	-0,657	4	-0,952	-0,634
SW	4	-0,566	-0,961	9	-0,134	-0,797
W	11	0,885	-0,139	18	0,819	-0,638
NE	5	-0,310	-0,635	8	0,859	-0,598
ANE	4	-0,922	0,107	4	-0,965	0,100
E	5	0,253	-0,638	5	0,893	0,336

For the AC circulation type, there is a high positive correlation between temperature and parameter C, ranging from 0.7% to 0.9% in 5 out of the 6 possible cases for Borovets and Moussala, including minimum, maximum, and mean nightly values of temperature and CCN. Only for the minimum values of temperature and C obtained from the minimum concentration of CCN on Moussala, the correlation coefficient is lower, 0.64%, which corresponds to a

moderate positive correlation. The correlation coefficient between parameter k and temperature (minimum, maximum, mean nightly) is low for all six cases for Moussala and Borovets.

In the W circulation type, the correlation coefficient between temperature and parameter C shows high positive correlation again in five out of six cases for Moussala and Borovets. These are again for the maximum and mean nighttime values of the parameter C and the maximum and mean nighttime temperatures at the Mt. Moussala, with values of 0.885% and 0.747%, respectively. For Borovets, these are for the values of parameter C obtained from the minimum, maximum, mean nighttime values of CCN concentration, and minimum, maximum, and mean nighttime temperature in Borovets, with values of 0.768%, 0.819%, 0.827%.

According to the Pearson correlation coefficient [47] a very high positive (negative) correlation is present when the values are between 0.90% and 1.00% (-0.90% and -1.00%). There are a total of 14 such cases for the correlation coefficient between parameter C and temperature at Moussala and Borovets during the study period. The correlation coefficient between parameter k and temperature at Moussala and Borovets has a very high negative correlation only in one of the cases during the study period: at the maximum temperatures at Moussala, it is -0.961% for SW.

7.4. Dependency between parameter C and temperature for AC and W circulation types according to JCT.

The most common weather types during the study period are anticyclonic (AC) and western (W) circulation types according to JCT. Each of them occurs 18 times. The dependence between parameter C from the Twomey equation, obtained from the maximum and nocturnal average concentration of pollutants and the corresponding maximum and nocturnal average temperature in the cases of the AC type for Mt. Moussala is presented in **Figure 7.3**, a). The dependence between parameter C from the Twomey equation, obtained from the minimum concentration of pollutants and minimum temperature in the cases of the AC type for Mt. Moussala is missing from **Figure 7.3**, because the correlation coefficient is low compared to the others. The dependence between parameter

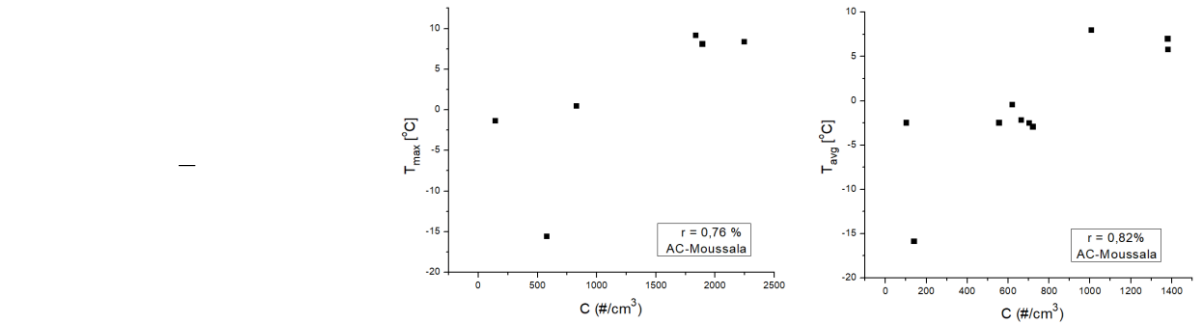

a)

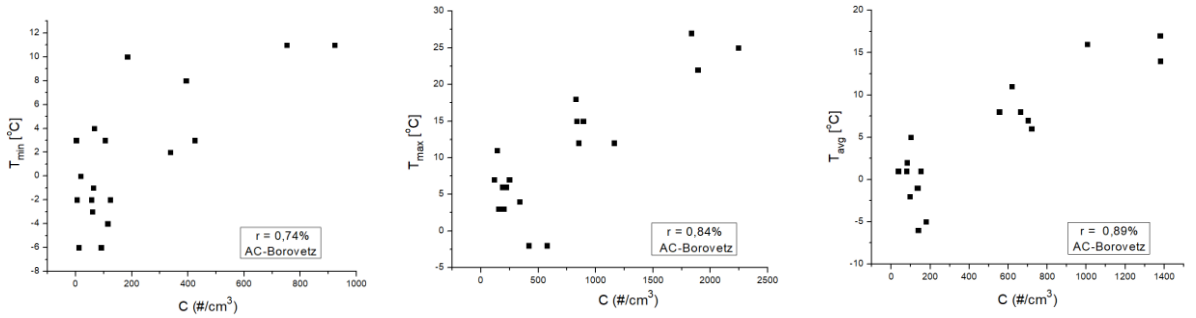

b)

Figure 7.3: Dependency between parameter C and Twomey equation obtained from minimum, maximum, and average nighttime concentration of CCN and corresponding temperature for AC type of circulation along JCT for *a)* Moussala and *b)* Borovets.

C from the Twomey equation, obtained from the minimum, maximum, and nocturnal average concentration of pollutants and corresponding minimum, maximum, and nocturnal average temperature in the cases of the AC type for Borovets is presented in Figure 7.3, b).

It can be seen in it that three clusters of points are formed, both at Mt. Moussala and in Borovets, with the strongest ones being expressed in the maximum and nocturnal temperatures in Borovets, **Figure 7.*3***, *b),* second and third panel.

7.5. Dependency between parameter C and temperature at the highest correlation coefficients.

From **Table 7.1** it can be seen that parameter C correlates more strongly (than parameter k) with temperature, both at the Moussala meteorological station and at the Borovets climatic station. **Figure 7.4** shows the dependencies between parameter C and temperature T in cases of the highest obtained correlation coefficients, on the first row for Moussala and on the second row for Borovets.

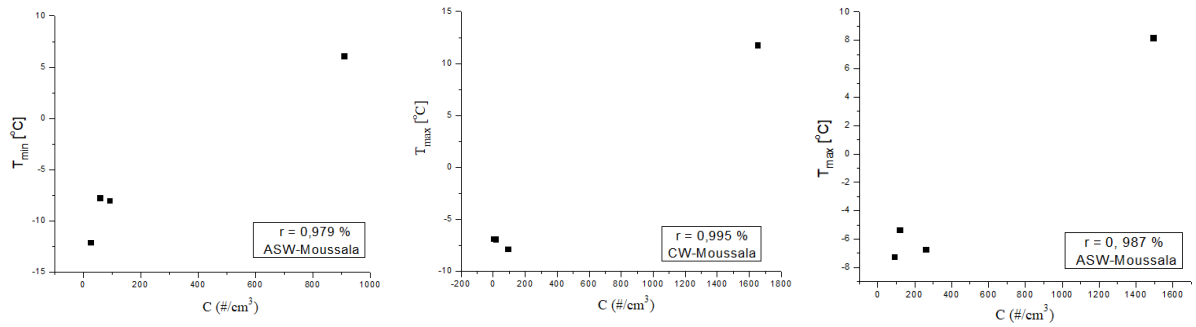

a)

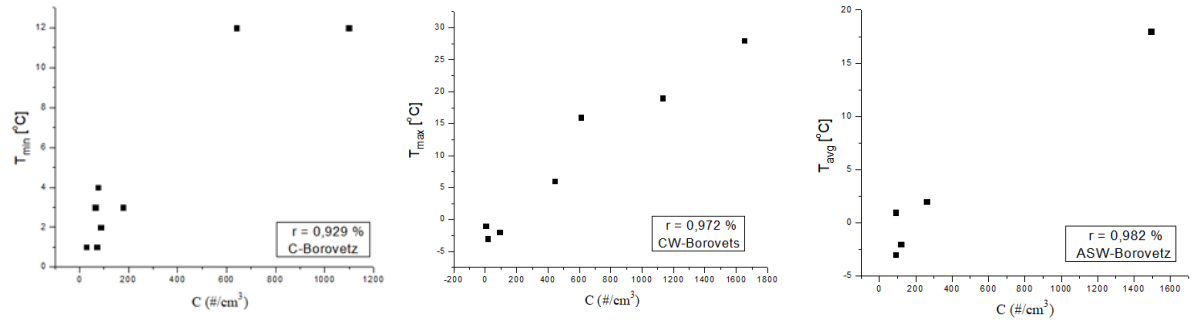

b)

Figure 7.4: Dependency of parameter C from the Twomey equation, obtained from the minimum, maximum, and average nighttime concentration of atmospheric pollutants and the corresponding temperature in the cases of the highest correlation coefficients, obtained for a) Moussala and b) Borovets.

From **Figure 7.4**, a) and b) it can be seen that the data for Moussala are significantly fewer in number than those for Borovets when the highest correlation coefficients are obtained. While at the Moussala meteorological station, two clusters of points are distinguished, similar to **Figure 7.3**, where three clusters of points are distinguished, the data from the Borovets climatic station lie in a curve which can be described by a third-degree polynomial.

Chapter 8

Analysis of data from heterogeneous nucleation

This chapter is dedicated to the (re-) analysis of data from precise experiments on heterogeneous nucleation in electrochemical conditions - electrodeposition of mercury (Hg) on two different types of Pt cathodes [36]. The authors specifically point out the analogy with vapor deposition on solid surfaces (due to the assumption that both cases involve nucleation mediated by so-called "active sites"), once conceptually and once when defining saturation in their system and the analogy with saturated vapors. It is part of a study that is under review.

8.1. Model α_{21}

The so-called α21 model in the context of two-dimensional crystallization with depletion of the initial supersaturation α_{21} [49] is given by:

$$n(t) = n_{max}\tanh^2(\frac{2t}{\tau_{21}}) \tag{8.1}$$

After approximating the data from figures 5 and 6 in Markov and Stoycheva [36] the scaling operation can also be viewed as a formulation of the "degree of conversion", as shown in **Figure 8.1**.

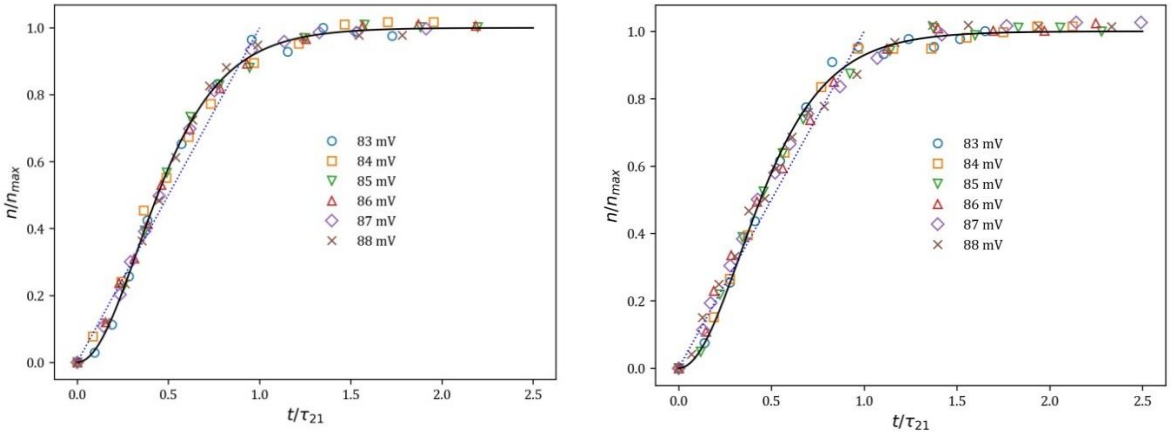

a) b)

Figure 8.1: Scaling of the data from a) Figure 5 and b) Figure 6 from Markov and Stoycheva [36] with the parameters obtained from fitting with Equation (8.1). The dashed line is the line of points $n/n_{max} = t/\tau_{21}$, while the solid curve is the universal (master) curve $n/n_{max} = \tanh^2(2t/\tau_{21})$.

Ideally, all scaled data should "collapse" onto the same universal curve, and the failure of a data set to do so should be considered a failure of the model to adequately describe that particular realization of the experiment. An important aspect in favor of α_{21} is that it does not have a "tuning" exponent, as the other two in the hierarchy do. As a result, only α_{21} has a universal curve of$n/n_{max} = \tanh^2(2t/\tau_{21})$, while for the other two models, the "universal" curves are as many as the values obtained for *d* and *q*, and in the Richards model, there is even one more – the dimensionless constant *K*.

8.2 Johnson-Mehl-Avrami-Kolmogorov's model

This is the most commonly used model in the studies of crystallization and nucleation, introduced as early as the 1930s by Kolmogorov [50], Johnson и Mehl [51], and Avrami [52].

$$n = n_{\max}\left\{1 - \exp\left[\left(2t / \tau_{\text{JMAK}}\right)^{d}\right]\right\} \tag{8.2}$$

In JMAKd, an additional parameter - the exponent d - appears, whereas in the original version of the model from the 1930s, it represents the dimensionality of the space in which recrystallization of alloys with a fixed number of nuclei occurs or the same plus one when it occurs under conditions of continuing nucleation, i.e., d is originally an integer number equal to 1, 2, 3, or 4. Over the years and with the distancing from the context in which the model was proposed, d began to be viewed as an additional parameter to improve the accuracy of the description, and when it is not an integer number, additional considerations are developed as to why it is not. Later, with the appearance of new data on non-integer degrees, the understanding of d evolves.

The relationship between the model and the previous one - α_{21} [49], expressed through the ratio of the two time scales - τ_{21} and τ_{JMAK} is the so-called conversion factor $c_f = \tau_{\text{JMAK}}/\tau_{21}$. In [49] it is shown that $\tau_{\text{JMAK}} \approx 1.1\tau_{21}$, when approximating data where the degree of transformation α tends towards 1.

The coefficient 2 in front of the time t in both models, equations (8.1) and (8.2), is used for convenience - then the inflection points of the rescaled model are "close" to the line $n/n_{max} = t/\tau$. The application of the JMAKd model is presented in Figure 8.2, using the Avrami plot of the data from Figure 8.1 a) and b), along with two specific values of d.

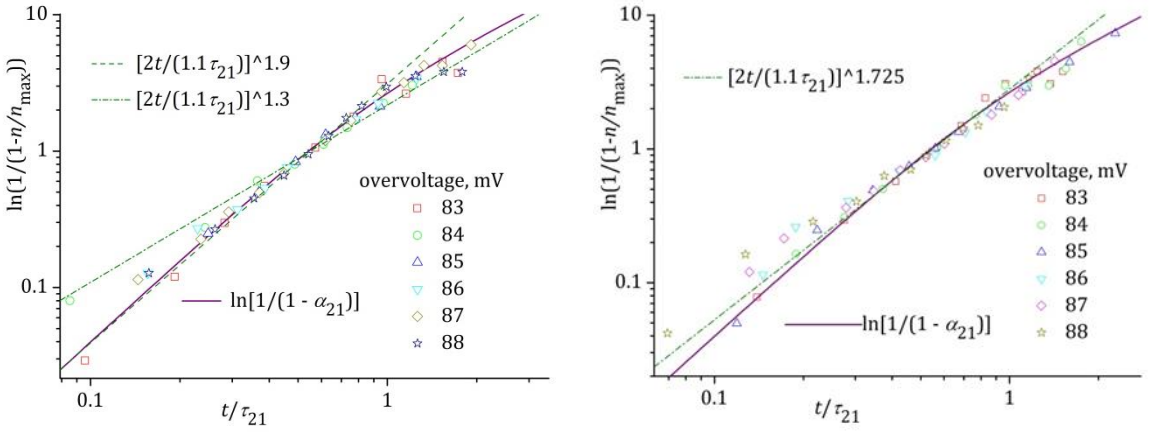

a) b)

Figure 8.1: Avrami plot of the rescaled data from a) Figure 8.1, a) and b) Figure 8.1, b) together with two specific values of d.

8.3. Richards model

The Richards model is another general model for studying growth [53], leading to a sigmoidal dependence due to the combined action of two feedback mechanisms - positive and negative (the form of the differential versions of the two models described above is also discussed and studied in [54]. The model is expressed by:

$$n(t) = \frac{n_{\max}}{\left(1+(q-1)\exp\left(-(t-t_i)/t_k\right)\right)^{(1/(q-1))}} \tag{8.3}$$

This model already has 4 parameters – $n_{\max}$, t_i – the time to reach the inflection point of the sigmoidal dependence, where the superlinear regime is replaced by the sublinear one, that is, the negative feedback "prevails", t_k - related to the kinetics of the process and the generalized power q. The scaling of the data from figures 5 and 6 of Markov and Stoicheva [36] is analogous here.

The Richards model has two commonly used special cases - the logistic model of Verhulst [55] - with q = 2, used in the context of nucleation by Nanev et al. [54], and the Gompertz model [56] - c q = 1, which are shown in *Figure* 8.2.

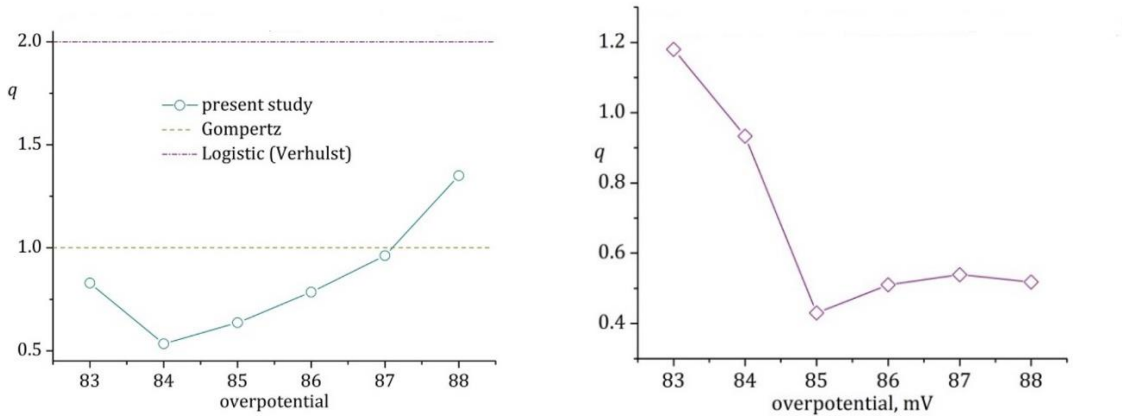

a) b)

Figure 8.2: Values of the tuning parameter q from the Richards model when applied to a) Figure 5 and b) Figure 6 of Markov and Stoycheva [36].

A description was presents of the procedures for data fitting and primarily the results obtained for α21, while the other two models serve more as confirmation of the results from the

simplest model. The most important result is presented in Figure 8.4 - the behavior of the two scales, in terms of the number of nuclei and time, as a function of overvoltage (supersaturation).

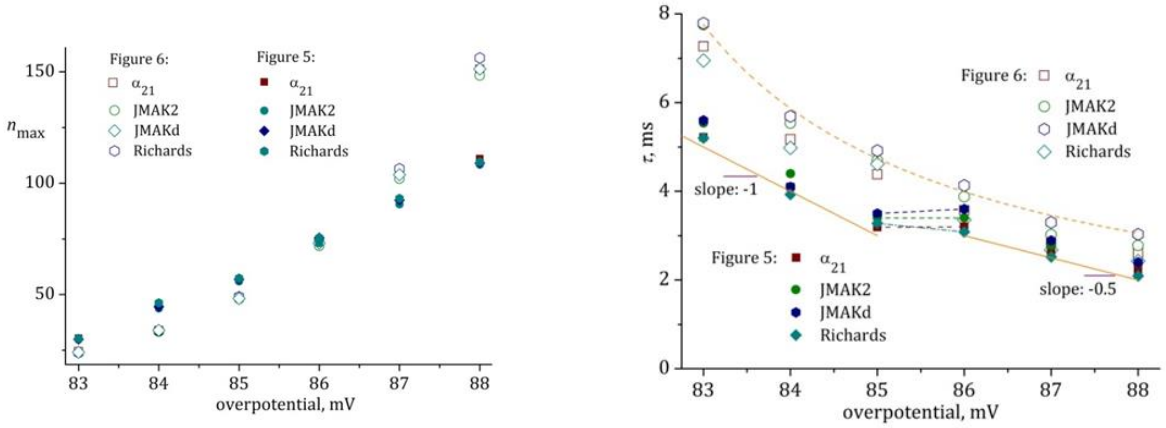

а) б)

Figure 8.3: Dependence of the obtained from modeling in this chapter the data from Markov and Stoycheva [36] scales for time and number of nuclei on the overvoltage (saturation) for a) nmax and b) for τ.

Chapter 9

CONCLUSIONS

The current dissertation work aims to develop a comprehensive approach to the study of atmospheric aerosols, particularly Cloud Condensation Nuclei (CCN), by placing the quantitative data on CCN obtained from the BEC Moussala (since 2016) in a broader meteorological context and seeking dependencies with measurable parameters from it.

To achieve this goal, the behavior of Cloud Condensation Nuclei (CCN) in different synoptic situations has been studied, on a daily and monthly scale. To obtain a good description of CCN, a detailed literature review was conducted, described in CHAPTER 2. Additional data were also used - synoptic classifications (Stefanov et al [40], Jenkinson-Collison-Types [43]), data from the HYSPLIT model [39], maps from the Global Forecast System GFS [44,57], NCEP/NCAR reanalysis [42], meteorological data from the Moussala synoptic station of NIMH (wind direction and speed, temperature), and the Twomey effect [16].

From the analysis of specific synoptic situations, it becomes clear that there is an extreme of CCN when a baric trough approaches or influences the region, associated with cyclonic activity whose main centers are far north or northwest of the Balkans. In the analyzed synoptic situations, these centers are over the northern part of the Scandinavian Peninsula and

west of the Norwegian coast, over the Atlantic Ocean. In addition, in such synoptic situations, the relative humidity of the air in the Mt. Moussala area is between 30 and 60%. Despite the large amount of CCN (especially in the situation examined in July), the visibility in the Moussala Observatory is very high - around 70 km for both situations. The prevailing wind directions are from the west quadrant during the winter situation and from the north quadrant during the summer situation, with better synchronization between the reported wind speeds in the two independent measurements in the second situation, during the summer half of the year.

When examining on a monthly scale, the results show that the concentration of air pollutants during the summer is much higher than during the winter (up to 4-5 times). The distributions of air pollutants, measured for six different concentrations (S) (0.13%, 0.23%, 0.43%, 0.63%, 0.83%, 1.03%), are transformed into their universal forms by scaling the number for each box to the total number of all boxes. Three main particle sizes of air pollutants are separated from the total of twenty: at 2 μm, 3 μm, and 5.5 μm. This allows for the identification of the scaling factor, representative of specific distributions, and then to investigate its behavior (when transformed as a concentration) instead of examining all distributions (one number instead of twenty). Clear extremes are distinguished in July: on the 5^{th} and 6^{th}, taken as one synoptic situation, and 13th (maximuma), and 18th (minimum), while in December there are three clear maximums on the 2^{nd}, 6^{th}, and 12^{th}. These days are examined in detail by searching for the influence of geopotential, temperature, and wind at 700 hPa, a height that corresponds approximately to the height of Mt. Moussala, on the distribution of air pollutant size. It has been found that the concentration maxima of air pollutants in July correspond to a geopotential gradient-free field at 700 hPa, while in December the Balkan Peninsula is influenced by a baric troughs.

In addition, the backward trajectories of air masses that influence Mount Moussala have been studied. They were calculated for 72 hours prior to reaching the peak, using the HYSPLIT model developed by NOAA. Based on the time spent by the air masses over the corresponding underlying surface, two main types of backward trajectories are identified, maritime and continental, with continental air masses predominating in both months, 30 days in July and 21 days in December, respectively.

The next subgrouping was based on a scheme for synoptic classification of atmospheric processes in the Balkan region. This scheme includes four types: Atlantic, continental, Mediterranean, and a gradientless baric field. Separation based on the thickness of the

atmospheric layer through which the air masses pass has also been used - low, medium, and high layer.

Reported are also all days with extreme values of the OKYA concentration. On these days, the prevailing atmospheric circulations according to JCT with 26 types during the OKYA minimums are C, NW, and W, and during the maximums, these are SW, W, and NW, with the first type being the most predominant in both cases. At extremely high values of the OKYA concentration, there are also three secondary types - AW, N, and NE. At extremely low values of the OKYA concentration, during atmospheric circulations of type C and NW, the predominant type of origin of the air mass is Sa and Cc, respectively. At extremely high concentrations of OKYA, the most commonly encountered air masses are two types: (1) that coming from the low layers (L) and is purely continental (Cc) and (2) that coming from the middle layers of the atmosphere (M) and has spent more than 75% of the time over the continent (Cb).

The Twomey law [16], (equation 2.3) was applied, which contains the concentration of CCN at a given saturation ratio S and two parameters, C and k. Parameter C is equal to the number of activated CCN at S=1% (#/cm^3), and parameter k is dimensionless and represents the rate of change of CCN with a change in saturation ratio. To determine the parameters of the law, an approximation of the data was made using the free software, for the minimum, maximum, and average daily values of CCN concentration in the BEO Moussala.

High correlation coefficients have been established between parameter C obtained from the minimum, maximum, and average daily concentration of CCN and the minimum, maximum, and average daily temperature at the Moussala synoptic station and the Borovets climate station. Borovets was chosen for comparison due to its location at the foot of the Mt. Moussala. Borovets is located at an altitude of 1350 m and is 10.3 km north of the Mt. Moussala in a straight line. The correlation coefficient for Moussala between temperature and parameter C has a very high positive correlation in 8 cases and a very high correlation in 11 cases out of all possible 36. The correlation coefficient for Borovets between temperature and parameter C has a high positive correlation in 17 cases and a very high correlation in 9 cases out of all possible 36.

Chapter 10

Scientific contributions, publications, and presentation of the results of the dissertation.

10.1. Scientific contributions of the dissertation

- A correlation has been established between the maxima in the concentration of atmospheric aerosols, the backward trajectories of air masses, and the synoptic conditions during 2016;
- Dependencies have been found between the extremes in the concentration of aerosols and the types of Jenkinson-Collison-Types circulation;
- High correlation coefficients have been found between a parameter from Twomey's equation and the temperatures at Moussala and Borovets;
- A jump in the time scale from one nucleation mode to another is obtained

10.2. Dissertation Publications

10.2.1. Journal publications with ISI impact factor

1) V. Kleshtanova, V. V. Ivanov, F. Hodzhaoglu, J.E. Prieto, V. Tonchev, Model hierarchy to reanalyze results from an archetypical experiment on the kinetics of heterogeneous nucleation - the electrodeposition of Hg on Pt, by I. Markov and E. Stoycheva. Crystals (MDPI) Preprint.

2) Kleshtanova, V., Tonchev, V., Angelov, Ch.: Extremes in the concentrations of CCN at Mt. Moussala and synoptic classifications, Proceedings of the Bulgarian Academy of Sciences, 2023, accepted for publication.

3) Kleshtanova, V., Stoycheva, A., Tonchev, V., Angelov, Ch.: Cloud condensation nuclei and backward trajectories of air masses at Mt. Moussala in two months of 2016, Journal of Atmospheric and Solar-Terrestrial Physics, 2023. https://doi.org/10.1016/j.jastp.2023.106004

4) Kleshtanova, V., Angelov, Ch., Kalapov, I., Arsov, T., Guerova, G., Tonchev, V. What one can learn from the cloud condensation nuclei (CCN) size distributions as monitored by the BEO Moussala?, AIP Conference Proceedings. 2019. https://doi.org/10.1063/1.5091311

10.2.2. Journal publications without ISI impact factor

1) Kleshtanova, V., Stoycheva, A., Tonchev, V.: Distributions of cloud condensation nuclei related to two synoptic situations in 2016. Bulgarian Journal of Meteorology and Hydrology 23, 17–30., 2019. http://meteorology.meteo.bg/global-change/files/2019/BJMH_2019_V23_N1/BJMH_V_Kleshtanova.pdf

10.2.3. Publications outside the topic of the dissertation

1) Kleshtanova, V., Markova, B., Kirilova, A.: Heavy rainfall in Karlovo valley in September 2022, Bul. J. Meteo & Hydro. http://meteorology.meteo.bg/global-change/files/2022/BJMH_2022_V26_N1/BJMH_26_1_3.pdf

10.3. Participation in projects

10.3.1. Head of a scientific project financed by Bulgarian sources

1) Analyzing extremely high concentrations of cloud condensation nuclei on Mount Moussala in 2017. First stage of national program "Young scientists and postdoctoral students - 2, ongoing. *In Bulgarian.*

2) Influence of air masses on cloud condensation nuclei. Third stage of the National Program "Young scientists and postdoctoral students", 2021, completed. *In Bulgarian.*

3) Distributions of cloud condensation nuclei and relation to two synoptic conditions in 2016. First stage of National Program "Young scientists and postdoctoral students", 2019, completed. *In Bulgarian.*

10.3.2. Participant in a scientific project financed by Bulgarian sources

1) How are synoptic maps developed?. H2020-MSCA-NIGHT-2020bis-101036078, K-TRIO 5, 2021.

2) Cloud condensation nuclei. Research project in support of doctoral students, supervised by Assoc. Ph.D. Veselin Tonchev. 80-10-192/27.04.2020 with FNI - SU.

10.3.3. Participant in a scientific project funded by foreign sources

1) COST inDUST “International Network to Encourage the Use of Monitoring and Forecasting Dust Products” – International Network to Promote the Use of Atmospheric Dust Monitoring and Forecasting Products. COST, CA16202.

10.4. Presentation of the results of the dissertation

10.4.1. Presentation of results at scientific forums

1) Kleshtanova, V: Air masses and cloud condensation nuclei on Mount Moussala. 4th Scientific Seminar "Physics and Chemistry of the Earth, the Atmosphere and the Ocean", Banya village, commune. Razlog, 9-11.10.2022. Report.

2) Kleshtanova, V: Cloud condensation nuclei from marine and continental air masses. 3rd Scientific Seminar "Physics and Chemistry of the Earth, the Atmosphere and the Ocean", Banya village, commune. Razlog, 3-5.10.2021. Report.

3) Victoria Kleshtanova, Saharan dust transport at BEO Moussala in 2016, Training School on dust products, NIMH, 27.01-29.01 2020. Report.

4) Kleshtanova, V., Stoycheva, A., Tonchev, V.: Distributions of cloud condensation nuclei and connection with two synoptic conditions in 2016. 2nd scientific seminar "Physics and Chemistry of the Earth, Atmosphere and Ocean", Pchelin, Kostenets, 13 - October 15, 2020. Report.

5) Kleshtanova, V., Angelov, Ch., Kalupov, I., Arsov, T., Gerova, G., Tonchev, V. Study of cloud condensation nuclei based on data from BEO Moussala and tracing their path along backward trajectories, VIII National student scientific conference on physics and engineering technologies, Park-hotel "Saint Petersburg", Plovdiv, 31.10 - 1.11.2019. Poster.

6) Kleshtanova, V.: Seasonal trend of cloud condensation nuclei in BEO Moussala. Training seminar physics and chemistry of the earth, the atmosphere and the ocean, Varshets, 31.05 - 2.06.2019., report.

10.4.2. Presentations outside of the dissertation topic

1) Kleshtanova, V.: Basic Environmental Observatory „Moussala”, First ACTRIS cloud in situ (CIS) community meeting, 01.12.2020, virtual, oral.

2) Kleshtanova, V.: Saharan dust transport at BEO Moussala in 2016, 6. Staubtag, Karlsruhe, Germany. 2019., oral.

BIBLIOGRAPHY

[1] Forster, P., Storelvmo, T., Armour, K., Collins, W., Dufresne, J.-L., Frame, D. et al. (2021) The Earth’s energy budget, climate feedbacks, and climate sensitivity. In Climate Change 2021: The Physical Science Basis Contribution of Working Group I to the Sixth Assessment

Report of the Intergovernmental Panel on Climate Change Cambridge University Press, Cambridge, United Kingdom and New York, NY, USA, Pp 923–1054,. https://doi.org/10.1017/9781009157896.009.

[2] Boucher, O., Randall, D., Artaxo, P., Bretherton, C., Feingold, G., Forster, P. et al. (2013) Chapter 7: Clouds and Aerosols. Climate Change 2013 the Physical Science Basis: Working Group I Contribution to the Fifth Assessment Report of the Intergovernmental Panel on Climate Change,. https://doi.org/10.1017/CBO9781107415324.016

[3] Boucher, O. and Boucher, O. (2015) Atmospheric aerosols. Springer. https://doi.org/10.1007/978-94-017-9649-1_2

[4] Tomasi, C. and Lupi, A. (2017) Primary and secondary sources of atmospheric aerosol. Atmospheric Aerosols: Life Cycles and Effects on Air Quality and Climate, Wiley Online Library. 1–86. https://doi.org/10.1002/9783527336449.ch1

[5] Pöschl, U. (2005) Atmospheric aerosols: Composition, transformation, climate and health effects. Angewandte Chemie - International Edition, 44. https://doi.org/10.1002/anie.200501122

[6] Mallet, M., Solmon, F., Nabat, P., Elguindi, N., Waquet, F., Bouniol, D. et al. (2020) Direct and semi-direct radiative forcing of biomass-burning aerosols over the southeast Atlantic (SEA) and its sensitivity to absorbing properties: a regional climate modeling study. Atmospheric Chemistry and Physics, Copernicus GmbH. 20, 13191–216. https://doi.org/10.5194/acp-20-13191-2020

[7] Lohmann, U. and Feichter, J. (2005) Global indirect aerosol effects: a review. Atmospheric Chemistry and Physics, Copernicus GmbH. 5, 715–37. https://doi.org/10.5194/acp-5-715-2005

[8] Paramonov, M. (2015) Life cycle of a cloud condensation nucleus, CCN. Helsingin yliopisto.

[9] McFiggans, G., Artaxo, P., Baltensperger, U., Coe, H., Facchini, M.C., Feingold, G. et al. (2006) The effect of physical and chemical aerosol properties on warm cloud droplet activation. Atmospheric Chemistry and Physics, 6. https://doi.org/10.5194/acp-6-2593-2006

[10] Andreae, M. and Rosenfeld, D. (2008) Aerosol–cloud–precipitation interactions. Part 1. The nature and sources of cloud-active aerosols. Earth-Science Reviews, Elsevier. 89, 13–41. https://doi.org/10.1016/j.earscirev.2008.03.001

[11] Hoppel, W., Frick, G. and Fitzgerald, J. (1996) Deducing droplet concentration and supersaturation in marine boundary layer clouds from surface aerosol measurements. Journal of Geophysical Research: Atmospheres, Wiley Online Library. 101, 26553–65. https://doi.org/10.1029/96JD02243

[12] Gautam, A.S., Tripathi, S., Joshi, A., Mandariya, A.K., Singh, K., Mishra, G. et al. (2021) First surface measurement of variation of Cloud Condensation Nuclei (CCN) concentration over the Pristine Himalayan region of Garhwal, Uttarakhand, India.

Atmospheric Environment, Elsevier. 246, 118123. https://doi.org/10.1016/j.atmosenv.2020.118123

[13] Rose, D., Nowak, A., Achtert, P., Wiedensohler, A., Hu, M., Shao, M. et al. (2010) Cloud condensation nuclei in polluted air and biomass burning smoke near the mega-city Guangzhou, China–Part 1: Size-resolved measurements and implications for the modeling of aerosol particle hygroscopicity and CCN activity. Atmospheric Chemistry and Physics, Copernicus GmbH. 10, 3365–83. https://doi.org/10.5194/acp-10-3365-2010

[14] Hoesly, R.M., Smith, S.J., Feng, L., Klimont, Z., Janssens-Maenhout, G., Pitkanen, T. et al. (2018) Historical (1750–2014) anthropogenic emissions of reactive gases and aerosols from the Community Emissions Data System (CEDS). Geoscientific Model Development, Copernicus GmbH. 11, 369–408. https://doi.org/10.5194/gmd-11-369-2018

[15] Köhler, H. (1936) The nucleus in and the growth of hygroscopic droplets. Transactions of the Faraday Society, Royal Society of Chemistry. 32, 1152–61. https://doi.org/10.1039/TF9363201152

[16] Twomey, S. (1959) The nuclei of natural cloud formation part II: The supersaturation in natural clouds and the variation of cloud droplet concentration. Geofisica Pura e Applicata, Springer. 43, 243–9. https://doi.org/10.1007/BF01993560

[17] Seinfeld, J. H. and Pandis, S. N. (1998): From air pollution to climate change. Atmospheric chemistry and physics, 1326.

[18] Detwiler, A., Langerud, D. and Depue, T. (2010) Investigation of the variability of cloud condensation nuclei concentrations at the surface in Western North Dakota. Journal of Applied Meteorology and Climatology, American Meteorological Society. 49, 136–45. https://doi.org/10.1175/2009JAMC2150.1

[19] Fang, S., Han, Y., Chen, K., Lu, C., Yin, Y., Tan, H. et al. (2016) Parameterization and comparative evaluation of the CCN number concentration on Mt. Huang, China. Atmospheric Research, Elsevier. 181, 300–11. https://doi.org/10.1016/j.atmosres.2016.07.004

[20] Hudson, J.G. (1980) Relationship between fog condensation nuclei and fog microstructure. Journal of Atmospheric Sciences, 37, 1854–67. https://doi.org/10.1175/1520-0469(1980)037<1854:RBFCNA>2.0.CO;2

[21] Martins, J.A., Gonçalves, F.L.T., Morales, C.A., Fisch, G.F., Pinheiro, F.G.M., Leal Júnior, J.B.V. et al. (2009) Cloud condensation nuclei from biomass burning during the Amazonian dry-to-wet transition season. Meteorology and Atmospheric Physics, Springer. 104, 83–93. https://doi.org/10.1007/s00703-009-0019-6

[22] Yang, S., Ma, J., Hu, Z., Yan, P., Chen, Y. and Wang, W. (2010) Influence of multi-chemical-component aerosols on the microphysics of warm clouds in North China. Science China Earth Sciences, 54. https://doi.org/10.1007/s11430-010-4075-z

[23] Raga, G. and Jonas, P. (1995) Vertical distribution of aerosol particles and CCN in clear air around the British Isles. Atmospheric Environment, Elsevier. 29, 673–84. https://doi.org/10.1016/1352-2310(94)00314-B

[24] Nilsson, E., Paatero, J. and Boy, M. (2001) Effects of air masses and synoptic weather on aerosol formation in the continental boundary layer. Tellus B, Wiley Online Library. 53, 462–78. https://doi.org/10.1034/j.1600-0889.2001.530410.x

[25] Liu, A., Wang, H., Li, Y., Yin, Y., Li, B., Chen, K. et al. (2020) Distribution characteristics of aerosol size and CCN during the summer on Mt. Tian and their influencing factors. Atmosphere, MDPI. 11, 912. https://doi.org/10.3390/atmos11090912

[26] Herenz, P., Wex, H., Mangold, A., Laffineur, Q., Gorodetskaya, I.V., Fleming, Z.L. et al. (2019) CCN measurements at the Princess Elisabeth Antarctica research station during three austral summers. Atmospheric Chemistry and Physics, Copernicus GmbH. 19, 275–94. https://doi.org/10.5194/acp-19-275-2019

[27] Hondula, D.M., Sitka, L., Davis, R.E., Knight, D.B., Gawtry, S.D., Deaton, M.L. et al. (2010) A back-trajectory and air mass climatology for the Northern Shenandoah Valley, USA. International Journal of Climatology: A Journal of the Royal Meteorological Society, Wiley Online Library. 30, 569–81. https://doi.org/10.1002/joc.1896

[28] Sogacheva, L., Hamed, A., Facchini, M., Kulmala, M. and Laaksonen, A. (2007) Relation of air mass history to nucleation events in Po Valley, Italy, using back trajectories analysis. Atmospheric Chemistry and Physics, Copernicus GmbH. 7, 839–53. https://doi.org/10.5194/acp-7-839-2007

[29] Soltani, M., Babu, C. and Mofidi, A. (2014) Meteorological aspects of an abnormal cooling event over Iran in April 2009. Meteorology and Atmospheric Physics, Springer. 124, 47–65. https://doi.org/10.1007/s00703-014-0309-5

[30] Tošić, I. and Unkašević, M. (2013) Extreme daily precipitation in Belgrade and their links with the prevailing directions of the air trajectories. Theoretical and Applied Climatology, Springer. 111, 97–107. https://doi.org/s00704-012-0647-5

[31] Yang, J., Lei, H. and Lü, Y. (2017) Airborne observations of cloud condensation nuclei spectra and aerosols over East Inner Mongolia. Advances in Atmospheric Sciences, Springer. 34, 1003–16. https://doi.org/10.1007/s00376-017-6219-y

[32] Yum, S.S., Hudson, J.G., Song, K.Y. and Choi, B. (2005) Springtime cloud condensation nuclei concentrations on the west coast of Korea. Geophysical Research Letters, Wiley Online Library. 32. https://doi.org/10.1029/2005GL022641

[33] Pérez, I.A., Artuso, F., Mahmud, M., Kulshrestha, U., Sánchez, M.L. and García, M.Á. (2015) Applications of air mass trajectories. Advances in Meteorology, Hindawi Limited. 2015, 1–20. https://doi.org/10.1155/2015/284213

[34] Scopus - Document search | Signed in [Internet].

[35] Kleshtanova, V., Angelov, C., Kalapov, I., Arsov, T., Guerova, G. and Tonchev, V. (2019) What one can learn from the cloud condensation nuclei (CCN) size distributions as monitored by the BEO Moussala? AIP Publishing LLC. p. 130026. https://doi.org/10.1063/1.5091311

[36] Markov, I. and Stoycheva, E. (1976) Saturation nucleus density in the electrodeposition of metals onto inert electrodes II. Experimental. Thin Solid Films, Elsevier. 35, 21–35. https://doi.org/10.1016/0040-6090(76)90237-6

[37] Milchev, A. and Montenegro, M.I. (1992) A galvanostatic study of electrochemical nucleation. Journal of Electroanalytical Chemistry, Elsevier. 333, 93–102. https://doi.org/10.1016/0022-0728(92)80383-F

[38] Basic Environmental Observatory - Moussala [Internet].

[39] Draxler, R.R. and Hess, G. (1997) Description of the HYSPLIT4 modeling system.

[40] Стефанов, С., Матеев, С., Лаловски, Х., Писарски, И., Кунчев, И. and Дончев, В. (1960) Proceedings of the Institute of Meteorology and Hydrology. Governmental publishing “Science and Art” 1–146.

[41] Stoev, K. and Guerova, G. (2020) Foehn classification and climatology in Sofia for 1975–2014. IDŐJÁRÁS/QUARTERLY JOURNAL OF THE HUNGARIAN METEOROLOGICAL SERVICE, Országos Meteorológiai Szolgálat. 124, 483–97. https://doi.org/10.28974/idojaras.2020.4.4

[42] 6-hourly NCEP/NCAR Reanalysis Composites: NOAA Physical Sciences Laboratory [Internet].

[43] Stoev, K., Post, P. and Guerova, G. (2022) Synoptic circulation patterns associated with foehn days in Sofia in the period 1979–2014. Quarterly Journal of the Hungarian Meteorological Service, 126, 545–66. https://doi.org/10.28974/idojaras.2022.4.5

[44] www.wetter3.de [Internet].

[45] Кръстанов, Л., Панчев, С. and Андреев, В. (1978) Обща метеорология. Наука и изкуство.

[46] Operator Manual: Cloud Condensation Nuclei (CCN-100) Counter – Single Column – Droplet Measurement Technologies [Internet].

[47] Swinscow, T.D.V. and Campbell, M.J. (2002) Statistics at square one. Bmj London.

[48] Hinkle, D.E., Wiersma, W. and Jurs, S.G. (2003) Applied statistics for the behavioral sciences. Houghton Mifflin college division. https://doi.org/10.2307/1164825

[49] Tielemann, C., Ivanov, V.I., Avramova, K., Reinsch, S. and Tonchev, V. (2023) Modelling crystallization: When transformation rate depends on the supersaturation.

[50] Kolmogorov, A.N. (1937) On the statistical theory of the crystallization of metals. Bull Acad Sci USSR, Math Ser, 1, 355–9.

[51] Johnson, W. and Mehl, R. (1939) Trans. AIME, p. 416.

[52] Avrami, M. (1939) Non-isothermal crystallization kinetics of poly (ethylene terephthalate) from the point of view of isokinetic models. J Chem Phys, 7, 1103–12.

[53] Tjørve, E. and Tjørve, K.M. (2010) A unified approach to the Richards-model family for use in growth analyses: why we need only two model forms. Journal of Theoretical Biology, Elsevier. 267, 417–25. https://doi.org/10.1016/j.jtbi.2010.09.008

[54] Nanev, C.N. and Tonchev, V.D. (2015) Sigmoid kinetics of protein crystal nucleation. Journal of Crystal Growth, Elsevier. 427, 48–53. https://doi.org/10.1016/j.jcrysgro.2015.07.007

[55] Verhulst, P.-F. (1838) Notice sur la loi que la population suit dans son accroissement. Corresp Math Phys, 10, 113–26.

[56] Gompertz, B. (1825) XXIV. On the nature of the function expressive of the law of human mortality, and on a new mode of determining the value of life contingencies. In a letter to Francis Baily, Esq. FRS &c. Philosophical Transactions of the Royal Society of London, The Royal Society London. 513–83.

[57] www.wetterzentrale.de - Google Search [Internet].